ELECTRON BEAM ANALYSIS OF MINOR ELEMENT SITE OCCUPANCIES IN TERNARY, QUATERNARY AND HIGHER ORDER DUPLEX ($\gamma + \alpha_2$) TITANIUM ALUMINIDES

by

C.J. Rossouw, P.R. Miller, M.A. Gibson and C.T. Forwood.

CSIRO Materials Science and Technology, Private Bag 33,
Rosebank MDC, Clayton, Victoria 3169, Australia.

GRANT NO. F49620-96-1-0024

Division of
Materials Science and Technology

CSIRO
AUSTRALIA

ELECTRON BEAM ANALYSIS OF MINOR ELEMENT SITE OCCUPANCIES IN TERNARY, QUATERNARY AND HIGHER ORDER DUPLEX ($\gamma + \alpha_2$) TITANIUM ALUMINIDES

by

C.J. Rossouw, P.R. Miller, M.A. Gibson and C.T. Forwood.

CSIRO Materials Science and Technology, Private Bag 33,
Rosebank MDC, Clayton, Victoria 3169, Australia.

GRANT NO. F49620-96-1-0024

REPORT DOCUMENTATION PAGE

Form Approved
OMB No. 0704-0188

1. AGENCY USE ONLY (Leave blank)	2. REPORT DATE	3. REPORT TYPE AND DATES COVERED
	20 JAN. 1997	FINAL Dec. 1995 — Dec. 1996

4. TITLE AND SUBTITLE
Electron Beam Analysis of Minor Element Site Occupancies in Ternary, Quaternary and Higher Order Duplex ($\gamma+\alpha_2$) Titanium Aluminides.

5. FUNDING NUMBERS
F49620-96-1-0024

6. AUTHOR(S) C.J. Rossouw, P.R. Miller, M.A. Gibson, C.T. Forwood.

7. PERFORMING ORGANIZATION NAME(S) AND ADDRESS(ES)
CSIRO, MATERIALS SCIENCE & TECHNOLOGY
NORMANBY ROAD, CLAYTON VIC. 3169
AUSTRALIA.

8. PERFORMING ORGANIZATION REPORT NUMBER
C97-05

9. SPONSORING/MONITORING AGENCY NAME(S) AND ADDRESS(ES)
AIR FORCE OFFICE of SCIENTIFIC RESEARCH
110 Duncan Avenue, Suite B115
Bolling AFB DC 20332-0001

10. SPONSORING/MONITORING AGENCY REPORT NUMBER

11. SUPPLEMENTARY NOTES Nil.

12a. DISTRIBUTION/AVAILABILITY STATEMENT
Public availability without limitation
"Distribution Statement A. Approved for public release; distribution is unlimited."

12b. DISTRIBUTION CODE

13. ABSTRACT *(Maximum 200 words)*

Duplex gamma/alpha2 Ti-Al alloys containing minor alloying additions of V, Cr, Nb, Ta and their combinations have been examined by micro-analytical electron microscopy to determine quantitatively the extent to which the additional alloying atoms: partition between the gamma and alpha2 phases; affect the state of atomic order, and occupy either Ti or Al host sublattice sites. Partitioning between the gamma and alpha2 phases was determined using conventional energy-dispersive X-ray analysis. The state of atomic order for each alloy was determined from measurements of relative positions of the quantum lines of electron intensity present in diffracted beams of the higher-order Laue zones in convergent beam electron diffraction patterns. Site occupancies of alloying elements were determined by a new fully quantitative statistical method of atom location by channelling-enhanced micro-analysis. The method is computerised with automated control of the electron beam, collection and analysis of the X-ray intensity data contained in incoherent channelling patterns. To cater for analysis of multiple alloying additions within a host lattice, a full energy dispersive X-ray spectrum is recorded for each pixel in incoherent channelling patterns. This has enabled the investigation of cross-elemental effects on atomic site occupancy.

14. SUBJECT TERMS	15. NUMBER OF PAGES
Titanium aluminides, site occupancy, duplex gamma/alpha2 alloys, statistical ALCHEMI, incoherent channelling pattern.	47
	16. PRICE CODE

17. SECURITY CLASSIFICATION OF REPORT	18. SECURITY CLASSIFICATION OF THIS PAGE	19. SECURITY CLASSIFICATION OF ABSTRACT	20. LIMITATION OF ABSTRACT
UNCLASSIFIED	UNCLASSIFIED	UNCLASSIFIED	

ABSTRACT

Duplex γ/α_2 Ti-Al intermetallic alloys containing minor ternary, quaternary and quinternary alloying additions of V, Cr, Ta, Nb and their combinations have been examined by analytical electron microscopy and diffraction to investigate the extent to which the additional alloying atoms (a) partition between the γ and α_2 phases, (b) affect the state of atomic order and (c) distribute themselves over Ti and Al host sublattice sites, and whether interstitial sites are occupied. Compositions and relative partitioning of the minor constituents between the γ and α_2 phases was determined using energy-dispersive X-ray analysis with full correction for X-ray absorption. The state of atomic order for each alloy was determined by a recently developed technique involving the measured positions of rocking curve maxima in diffracted beams from high order Laue zones when the crystal is in an appropriate symmetrical zone axis orientation. The position of each maximum is associated with one of the highly symmetric fast electron quantum states which discriminate between different projected scattering symmetries in the unit cell, and these are related to the degree of order. Atomic site occupancies of the additional alloying elements were determined by a quantitative statistical method for atom location by channelling-enhanced micro-analysis. This method has been developed with computerised control over both electron beam orientation and data collection in order to form incoherent channelling patterns from variations in characteristic X-ray intensities as a function of beam orientation. The system is deliberately configured to record the full X-ray spectrum for each pixel in the channelling pattern so as to allow the analysis of any number of alloying additions. This has enabled the investigation of cross-elemental effects, such as how atomic site occupancy of one particular alloying element is affected by the presence of a second or third element. Limitations of ALCHEMI analysis due to delocalisation of the ionization event, disorder and occupancy of interstitial sites are clarified by comparing experimental data with that computed using the theory of characteristic X-ray emission from absorptive crystals under dynamical electron diffraction conditions.

CONTENTS

1. Introduction

Ordered intermetallic alloys based on TiAl are currently being considered as potential engineering materials for applications where high strength, low density and good oxidation resistance at elevated temperatures are required (see Kim 1989, Kim and Dimiduk 1991 and Kim 1994). At room temperature the alloys are essentially brittle and this problem, coupled with the need to improve oxidation resistance, represent the major limitations to their practical application.

Titanium-rich compositions (e.g. $Ti_{52}Al_{48}$) with two-phase alloy structures are favoured because such structures can lead to improvements in mechanical properties over single-phase γ alloys. The two-phase structure consists of a mixture of a minority α_2-phase, based on Ti_3Al with the ordered hexagonal DO_{19} crystal structure, together with a majority γ-phase, based on TiAl with the ordered tetragonal $L1_0$ crystal structure. A range of differing microstructural morphologies can be established by appropriate heat treatments and optimum ductility is achieved with a duplex microstructure, which typically consists of lamellar ($\gamma+\alpha_2$) grains interspersed with γ grains and a low density of faceted α_2 grains. The lamellar ($\gamma+\alpha_2$) grains comprise alternate γ and α_2 lamellae (~1 μm across) with interfaces parallel to $(111)_\gamma/(0001)_{\alpha2}$; the orientation relationship being given by: $(111)_\gamma \parallel (0001)_{\alpha2}$ with $<1\bar{1}0>_\gamma \parallel <11\bar{2}0>_{\alpha2}$. The improvement in ductility in these duplex alloys stems from the generation under stress of enhanced deformation twinning and slip dislocation activity in the majority γ-phase which is considered to arise from the activation of dislocation sources associated with the γ/α_2 interfacial defect structure (see Appel, Beaven and Wagner 1993, and Wunderlich, Kremser and Frommeyer 1993).

Further improvements to ductility as well as to oxidation resistance have been achieved by the incorporation of additional alloying elements in the range 1 to 5 at.%. For example, V, Cr and Mn

have been found to improve room temperature ductility (see Huang and Hall 1991a & b, and Hanamura, Uemori and Tanimo 1988) and Nb and Ta to improve oxidation resistance (M^{c}Kee and Huang 1992). In order to gain an understanding of the role played by such extra alloying elements it would be necessary to consider their influence within the γ and α_2 phases on effects such as: electron bonding, phase equilibria, stacking fault energy, twin boundary energy, antiphase boundary energy and resistance to dislocation motion. However, such effects will depend strongly on:

(i) the extent to which the atoms of each alloying element are partitioned between the γ and α_2 phases;

(ii) the type of crystal lattice sites that are occupied by the additional alloying atoms (i.e. the extent to which alloying elements favour Ti or Al sublattice sites in the γ and α_2 phases); and

(iii) the degree to which atomic ordering within the two phases is affected by the presence of the extra alloying elements (Morinaga, Saito, Yukawa and Adachi 1990, and Xu and Freeman 1994).

For example, in the case of atomic site occupancy it has been demonstrated (Morinaga *et al* 1990) that if improvements to ductility brought about by the addition of V, Cr or Mn occur as a result of d-d electron bonding being enhanced at the expense of p-d bonding, then this can be only be achieved when the additional alloying atoms occupy Al (rather than Ti) sublattice sites. Thus, an investigation of the three atomic processes (i) - (iii) represents an initial step towards understanding the way in which minority alloying additions affect macroscopic properties, and this report describes such an investigation for a duplex $Ti_{52}Al_{48}$ alloy containing additions of V, Cr, Ta, Nb and their combinations.

It is shown that the degree to which the additional alloying elements partition between the γ and α_2 phases can be reliably determined using conventional energy-dispersive X-ray (EDX) analysis when due account is taken of the absorption of characteristic X-rays within the specimen.

Site occupancy of additional ternary elements in the γ-phase has been investigated by several workers using ratio techniques in conjunction with X-ray intensity measurements and atom location by channelling enhanced microanalysis (ALCHEMI) (Huang and Hall 1991a, Doi, Hashimoto, Kasahara and Tsujimto 1990, Shindo, Hirabayashi, Kawabata and Kikuchi 1986, Konitzer, Jones and Fraser 1986 and Mohandas and Beaven 1991). However, the results obtained have not been entirely consistent, e.g. V additions have been shown in one case to strongly favour Al sublattice sites and in another case to strongly favour Ti sublattice sites. A likely reason for such discrepancies lies with the effects that interaction delocalisation can have on ALCHEMI when the ratio method is used, particularly for the case of relatively low energy characteristic X-rays from Al, and the inability of the ratio method to provide reliable estimates of the errors incurred.

The ALCHEMI method for determining crystallographic site distributions of substitutional species within a host crystal was first developed by Taftø and Spence (1982) and Spence and Taftø (1983). The original method involved ratios of normalized X-ray count rates under differing dynamical diffraction conditions and proved successful in a number of studies (see for instance Krishnan 1988, Smyth and McCormick 1988). However, since low energy X-ray emissions are generally less responsive to changes in dynamical diffraction conditions than high energy X-rays due to interaction delocalization, the ratio method can lead to misleading results. The errors involved may be exceptionally large because ratios, involving differences in X-ray counts between a "channelling" and a "non-channelling" orientation, suffer from the disadvantage of amplifying errors, particularly when channelling effects are small (Rossouw, Forwood, Gibson and Miller, 1996a). To-date, attempts to correct for the effects of delocalization in the ratio ALCHEMI technique have not been generally applicable (Pennycook and Narayan 1985, Pennycook 1988, Rossouw, Turner and White 1988, Spence, Kuwabara and Kim 1988). For this reason an alternative method of obtaining and analysing data,

which is less sensitive to delocalization effects and capable of providing quantitative estimates of precision and errors limits, has been developed, based on the statistical method of ALCHEMI originally proposed by Rossouw, Turner, White and O'Connor (1989).

In this report the formulation of this new statistical method of analysis is presented, together with a description of the computerised method that has been developed for collecting the necessary experimental data from X-ray incoherent channelling patterns (ICPs), i.e. those patterns formed by the variation in characteristic X-ray emission as a function of crystal orientation with respect to the electron beam. It is shown that, by collecting a full energy dispersive X-ray spectrum as data at each pixel of the ICP, the method can be applied to the analysis of multiple alloying species within a host lattice.

This overall experimental and analytical procedure is applied to both the γ and α_2 phases in duplex Ti-Al alloys to determine the atomic site occupancy of ternary, quaternary and quinternary additions of V, Cr, Ta, Nb and their combinations, thus enabling an investigation of cross-elemental effects i.e. how site occupancy associated with one particular element is affected by the presence of other element additions.

In order to obtain a more complete understanding of the atomic structure within each alloy phase, it is necessary to make independent determinations of two additional factors; namely the extent to which atoms of the extra alloying elements: (i) occupy interstitial atomic sites, and (ii) affect the state of atomic order within the host lattice (Hou, Jones and Fraser, 1996). Both of these problems are addressed in this report.

The occupation of interstitial sites is determined from a direct comparison of experimental and theoretical ICPs. Theoretical ICPs are computed using dynamical electron diffraction theory in conjunction with recently-developed expressions for the ionization cross-section of atoms within an absorptive crystal. This enables enhancement factors for characteristic X-ray emission to be calculated which, not only include appropriately delocalized and thermally-smeared ionization potentials, but also take account of the absorption of characteristic X-rays within the specimen.

The state of atomic order in the γ-phase of each alloy is determined from convergent beam electron diffraction (CBED) patterns using the method recently developed by Rossouw, Gibson and Forwood (1996). The degree of order is obtained from measurements of the relative separation of different branches of the dispersion surface as observed in quantum state rings present in diffracted electron beams of higher order Laue zones (HOLZ) when the crystal is orientated at an appropriate symmetrical zone axis orientation.

2. Channelling Contrast

In this section the theory for the formation of X-ray ICPs is presented with due account being taken for the absorption of X-rays within the specimen so that it can be used as a basis for generating computer simulated ICPs that are directly comparable with those obtained experimentally.

It has been shown by Rossouw (1985) that the intensity of X-ray emission generated by a fast electron beam from a crystalline specimen by localized sources at points within each unit cell is proportional, by reciprocity, to the fast electron probability density at those points within the unit cell, averaged over the thickness of the specimen. The fast electron probability density may be derived from the dynamical wavefunction $\phi(\mathbf{r})$, which in turn is expressed as a sum of Bloch waves, i.e.

$$\varphi(r) = \sum_i \alpha^{(i)} \varphi^{(i)}(r) \qquad (1)$$

where $\alpha^{(i)}$ is the excitation amplitude of the quantum Bloch state $\phi^{(i)}(\mathbf{r})$, which is written as

$$\varphi^{(i)}(r) = \sum_g C_g^i \exp[\, i\, (k^i + g)\, r\,] \qquad (2)$$

where $\mathbf{g}$ is a reciprocal lattice vector multiplied by 2π and C_g^i is an eigenvector component of quantum state (i). $\mathbf{k}^i$ is the complex eigenvalue describing both propagation and absorption of this state on branch (i) of the dispersion surface and the absorptive component can be obtained directly from eigenanalysis of the interaction of the fast electron wavefunction with the combined elastic and absorptive potentials. Here, Fourier coefficients of the elastic scattering potential are derived from Doyle and Turner (1968) parameters for X-ray scattering of neutral atoms, and converted to electron scattering factors via the Mott formula. The Debye-Waller factors used for the γ-phase are $M_y = 8\pi^2 \langle u_y^2 \rangle$ and were measured at 100 K to be 0.305 Å^2 for Ti and 0.311 Å^2 for Al (Rossouw,

Gibson and Forwood, 1997). Since the α_2-phase has a fair amount of disorder due to composition being off-stoichiometry (i.e. an excess of Al atoms in the idealised $D0_{19}$ crystal structure), the Debye-Waller factors are fairly large due to a strain component, and assumed to be 0.5 $Å^2$ for all atoms in this phase. For the absorptive potential an Einstein model (Radi 1970, Allen and Rossouw 1989, Bird and King 1990) is used to describe thermal diffuse scattering, which provides a wide-angle 'dechannelling' mechanism for the fast electron.

The dynamical enhancement factor for X-ray emission from an atom of type y within an absorptive crystal is a function of beam direction (or equivalently crystal orientation) s, depth z of the atom within the crystal and absorptive processes for the fast electron (Allen and Rossouw 1993b; Josefsson, Allen, Miller and Rossouw 1994). This enhancement can be regarded as the factor that relates the interaction cross-section for X-ray emission from an atom under dynamical diffracting conditions to that under kinematical diffracting conditions. It is denoted as $F_y^s(z)$ and may be written as a sum of dynamic and kinematic components, $D_y^s(z)$ and $K_y^s(z)$, respectively (Rossouw, Forwood, Gibson and Miller 1996a; *Ibid* 1996b). Briefly, the dynamical component $D_y^s(z)$ is given by

$$D_y^s(z) = \sum_{ij} \alpha^i \alpha^{j*} \sum_{gh} C_g^i C_h^{j*} \frac{M_y(h,g)}{M_y(o,o)} e^{i(k^i - k^{j*})z} \qquad (3)$$

The term $M_y(\mathbf{h},\mathbf{g})$ includes transition matrix elements for inner shell ionization, appropriately distributed over interaction sites τ_n within the unit cell. Occupancies p_{ny} of various sites n by atoms of type y are included as

$$M_y(\boldsymbol{h},\boldsymbol{g}) = A_y(\boldsymbol{h},\boldsymbol{g}) \sum_n p_{ny} \exp[\, i(\boldsymbol{g}-\boldsymbol{h})\, \tau_n \,] \quad . \qquad (4)$$

Here $A_y(\mathbf{h},\mathbf{g})$ terms are related to Fourier coefficients of the non-local ionization potential (Josefsson *et al* 1994), determined by cross-products of non-diagonal transition matrix elements integrated over momentum and energy transfers for the (e,2e) event (Maslen and Rossouw 1984, Rossouw and Maslen 1984). If a local approximation is invoked, then $A_y(\mathbf{g},\mathbf{h}) = A_y(\mathbf{h}-\mathbf{g})$, and Fourier transforms of assumed Gaussian (Nuchter and Siegle 1995, Rossouw 1995) or Lorentzian interaction profiles (Rossouw *et al* 1996a), smeared by Debye-Waller factors, may be used in evaluating $A_y(g')$ where $g' = \mathbf{h}-\mathbf{g}$. For a local Lorentzian potential $A_y(x)$ of half-width b_y,

$$A_y(g') = [\frac{\pi \exp(-b_y g')}{b_y}] \quad [\exp(-\frac{1}{2}g'^2 \langle u_y^2 \rangle)] \quad , \tag{5}$$

where the first term enclosed in square brackets is the Fourier transform of the Lorentzian, thermal smearing is in the second term and $\langle u_y^2 \rangle$ is the mean square displacement of atom y from equilibrium (Allen and Rossouw 1993a; Cherns, Howie and Jacobs 1973).

Fast electrons, which have been dechannelled by localized thermal scattering processes or by inelastic electronic interactions, provide a kinematic component $K_y^s(z)$ to the generation of characteristic X-rays (an average over all wide angle scattering processes is assumed to provide a contribution similar to that of a plane wave). In the absence of absorption, Bloch eigenstates are normalized such that $\Sigma_g I_g(z) = 1$, where $I_g(z)$ is the intensity for a diffracted beam at a depth z. With absorption, the contribution from dechannelled electrons is thus $1 - \Sigma_g I_g(z)$. I_g may be written from Bloch wave coefficients as

$$I_g(z) = \sum_{ij} \alpha^i \alpha^{j*} \; C_g^i C_g^{j*} \; e^{i\,(k^i - k^{j*})\,z} \tag{6}$$

and the orthogonality condition $\Sigma_g C_g^i C_g^j = \delta_{ij}$ may be used in a summation over I_g to yield

$$K_y^s(z) = 1 - \sum_i \alpha^i \alpha^{j*} e^{i(k^i - k^{j*})z} \quad . \tag{7}$$

For convenience, we now relate the pathlength z' for X-ray absorption (i.e. the distance the photon travels through the specimen towards the detector) to the depth z at which the ionization event occurred. As shown in fig 1, z is the depth within the crystal along the direction of the incident beam. For the simple case of a detector with takeoff angle θ mounted at 90° to the tilt axis, with a uniform flat specimen being tilted by an angle ϕ towards the detector, $z' = Rz$ where $R = \cos \phi / \sin (\phi+\theta)$. Here the goniometer tilt angle is ϕ, and any tilt of the holder about an orthogonal axis has no effect on R. This formulation is readily extendable to an arbitrary detector and double-tilt holder configuration, as described by Horita, Sano and Nemoto (1991). Absorption of the emitted X-ray is accounted for by an extra attenuation term $\exp(-Rz/\lambda_y)$ on the dynamical enhancement factor. Here λ_y is the mean free path for absorption of X-rays from atom y within the specimen, $\lambda_y = 1/\mu_y\rho$, where μ_y is the mass absorption coefficient and ρ the density.

In order to simulate the formation of X-ray ICPs, it is necessary to obtain the thickness-integrated enhancement factor $F_y^s(t)$, with the effects of X-ray absorption included. To achieve this, terms in z are integrated and averaged over thickness t with the absorptive term included, i.e.

$$F_y^s(t) = \frac{1}{t} \int_0^t [\, D_y^s(z) + K_y^s(z) \,]\, e^{-Rz/\lambda_y}\, dz = D_y^s(t) + K_y^s(t) \quad . \tag{8}$$

The integration over z is obtained from the form

$$\frac{1}{t} \int_0^t e^{i\beta z}\, dz = \frac{e^{i\beta t} - 1}{i\beta t} \quad . \tag{9}$$

where β may be complex. Thus the dynamical component $D_y^s(t)$ from eqn. (3) becomes

$$D_y^s(t) = \sum_{ij} B_y^{ij}(t) \sum_{gh} C_g^i C_h^{j*} \frac{M_y(h,g)}{M_y(o,o)} \tag{10}$$

where $B_y^{ij}(t)$ is a Bloch wave interference term given by

$$B_y^{ij}(t) = \alpha^i \alpha^{j*} \frac{e^{i\Delta_y^{ij} t} - 1}{i\Delta_y^{ij} t} \quad , \tag{11}$$

where Δ_y^{ij} is defined as $k^i - k^{j*} + iR/\lambda_y$. The kinematic component $K_y^s(t)$ from eqn. (7) may be written

$$K_y^s(t) = \left[\frac{1 - e^{-Rt/\lambda_y}}{Rt/\lambda_y} \right] - \sum_i B_y^{ii}(t) \quad . \tag{12}$$

In the absence of diffraction, terms containing the Bloch wave interference term B_y^{ij} from dynamic and kinematic components cancel, and the remaining term within square brackets in eqn. (12) is the usual correction term to account for absorption of X-rays if diffraction is not considered (Goldstein, Costley, Lorimer and Reed, 1977). Additionally, as t increases well beyond the mean free path for dechannelling of the fast electrons, the dynamical enhancement factor $F_y^s(t)$, as expected, asymptotes to this term. Thus, values of $F_y^s(t)$ computed from eqns. (8)-(12) for a variation in incident electron beam direction, s, can be used to simulate an ICP, where the same variation in electron beam direction produces a variation in the characteristic X-ray emission from atoms of type y in a specimen of thickness t.

3. HOLZ Contrast

For an incident electron beam direction, **u**, (defined along the direction of electron flow) the nth order Laue zone is defined by a set of reciprocal lattice vectors, **g**, such that n = -**g**.**u**. It has been shown by Rossouw, Gibson and Forwood (1996) that, for the γ-phase of a Ti-Al alloy, three distinct rings are visible in diffracted beams in the n = 2 HOLZ of a <110] CBED pattern. Positions of these maxima are associated with the binding energy of the three highly symmetric fast electron quantum states $\phi^{(i)}(\mathbf{r})$ that are excited near the symmetrical zone axis orientation (the more tightly bound the quantum state, the smaller the Bragg angle for the associated HOLZ ring). The different quantum states discriminate between different projected scattering symmetries in the unit cell and these are related to the degree of order, so that the relative spacing between the rings provides a sensitive measure of atomic order. The atomic order parameter P in the γ-phase was determined by finding the value of P which gives calculated spacings between the three HOLZ rings that fit the spacings measured in experimentally obtained <110] CBED patterns.

For HOLZ calculations, full complex general solutions are required for the scattering matrix from which the wavefunctions in eqns. (1) and (2) are derived (Rossouw and Hampikian 1993), and exact eigenanalysis procedures for a complex general scattering matrix have been addressed by Allen and Rossouw (1989), allowing direct retrieval of HOLZ beam amplitudes without invoking renormalization techniques (Lewis, Villagrana and Metherell 1978).

It is interesting to note that, for the $L1_0$ crystal structure of the γ-phase, structure factors, $F_{hk\ell}$, for reflections with hkℓ all odd or even are insensitive to order, whereas $F_{hk\ell}$ for mixed odd and even hℓ or kℓ indices are related to differences in atomic scattering factor from Ti and Al sublattice sites.

For a partially ordered alloy, structure factors $F'_{hk\ell}$ with mixed indices are linearly related to the fully ordered values $F_{hk\ell}$ via the order parameter P, i.e.

$$F'_{hkl} = P\, F_{hkl} \qquad (13)$$

4. Statistical ALCHEMI Analysis

In this section the theoretical basis for the statistical method of ALCHEMI is presented, showing how the concentrations or distributions of minority alloying species on host atomic sites can be determined from experimental data in alloys which may be only partially ordered. In the following, the term 'host species' refers to atoms that are included in the general chemical formula from which the basic crystal structure is derived, and parameters that refer to these atoms are subscripted i. Additional minority alloying atoms that are accommodated on substitutional or interstitial sites within the unit cell, and related parameters bear the subscript x.

If host atoms of type i have an occupancy z_{ni} of available sites n = 1...N in the unit cell, then their concentration (prior to minority alloying atoms of type x being accommodated) is given by

$$c_y = \frac{1}{N} \sum_{n=1}^{N} z_{ny} \quad . \qquad (14)$$

The X-ray counts N_i^s from these host atoms under a particular dynamical diffraction conditions s may be written as

$$N_i^s = K_i \left(c_i - \sum_x c_x f_{ix} \right) F_i^s \qquad (15)$$

where the concentration of a minority alloying atom x is c_x, f_{ix} is the relative distribution of these minority species x over sites occupied by host atoms i, and F_i^s is the dynamical enhancement factor (as defined in §2), which includes effects of delocalization and thermal smearing, as discussed in §2. Note that partial occupancy of sites i by the minority atoms x is accounted for via the sum $\Sigma_x c_x f_{ix}$. For alloy systems which are *not* fully ordered or stoichiometric, the index i in the distribution f_{ix} refers both to atoms i on their preferred sites *and* anti-sites. ALCHEMI analysis as presented below is thus valid provided that occupation of sites by the additional alloying atoms in a non-stoichiometric or partially disordered system proceeds with the constraint that the ratio of site occupancies of the additional alloying elements compared with host species, z_{nx}/z_{ni}, is independent of site τ_n. This constraint in itself excludes the possibility of interstitial site occupancy by the minority alloy species. Thus a sum over available sites now effectively becomes a sum over substitutional sites. Returning to eqn. (15), K_i is a term given by

$$K_i = \frac{I_o N t}{V_c} (Q_i \omega_i a_i \varepsilon_i) \qquad (16)$$

where I_o is the beam intensity, t the specimen thickness, Q_i the ionization cross-section and ω_i the fluorescence yield. a_i is the fraction of the total X-ray line intensity that is measured, depending on the position and width of the energy window. ε_i is the detection efficiency and V_c the unit cell volume.

The X-ray counts N_x^s from the minority elements x may be written as

$$N_x^s = K_x \, c_x \sum_i f_{ix} \, F_{ix}^s \quad . \tag{17}$$

Now a crucial approximation is made: The dynamical enhancement factor F_{ix}^s for minority atoms x on sites i is assumed to be equal to F_i^s. This approximation is reasonable provided that the excitations responsible for the X-ray counts are localized compared with possible fluctuations in the fast electron probability density across the various sites. Substituting the value for F_i^s from eqn. (15) for F_{ix}^s in eqn. (17) yields

$$N_x^s = c_x \sum_i \frac{f_{ix} \, N_i^s}{k_{xi} \, (\, c_i - \sum_x c_x \, f_{ix} \,)} \tag{18}$$

where $k_{xi} = K_i/K_x$ is the atomic k-factor of element x relative to element i.

Following Rossouw *et al* (1989) and Turner *et al* (1991) the statistical approach to ALCHEMI analysis invokes the assumption that N_x^s may be written as a linear combination of N_i^s for each spectrum or channelling condition s. Thus

$$N_x^s = \sum_i a_{ix} \, N_i^s + C_x \quad . \tag{19}$$

where a_{ix} and C_x are coefficients to be determined. The constant offset C_x is included as an extra parameter (Rossouw *et al* 1996a) which, to some extent, accounts for differences in interaction delocalization (hence response to changing dynamical diffraction conditions) and errors in background subtraction, as well as allowing for the possibility that minority atoms may be in interstitial sites within the unit cell so as to give no correlation with host atom counts. It may also be considered simply as a 'fudge factor' which will be shown to provide better accuracy, despite one degree of freedom being lost in the analysis. Note that no distinction between 'channelling' and 'non-channelling' orientations

is made, the only requirement being that variation in orientation results in changes in relative X-ray intensities from the host sites.

Comparison between eqns. (18) and (19) allows coefficients a_{ix} to be identified as

$$a_{ix} = \frac{c_x f_{ix}}{k_{xi} (c_i - \sum_x c_x f_{ix})} \qquad (20)$$

and now it is necessary to express c_x and f_{ix} in terms of these coefficients. Firstly, the sum over additional minority atoms x for a particular host site i is evaluated, i.e.

$$\sum_x a_{ix} k_{xi} = \frac{\sum_x c_x f_{ix}}{(c_i - \sum_x c_x f_{ix})} \quad , \qquad (21)$$

which may be rearranged as

$$\sum_x c_x f_{ix} = \frac{c_i \sum_x a_{ix} k_{xi}}{(1 + \sum_x a_{ix} k_{xi})} \quad . \qquad (22)$$

Next, the summation in the numerator over x in eqn. (22) is dropped and replaced by a sum over i. Since $\Sigma_i f_{ix} = 1$, this yields

$$c_x = \frac{\sum_i c_i a_{ix} k_{xi}}{(1 + \sum_x a_{ix} k_{xi})} \qquad (23)$$

and the distribution between sites from eqn. (22) is

$$f_{ix} = \frac{c_i a_{ix} k_{xi}}{c_x (1 + \sum_x a_{ix} k_{xi})} \quad . \qquad (24)$$

Thus, for each minority alloy species, x, eqns. (23) and (24) enable the concentration c_x and distribution f_{ix} to be obtained from experimentally determined values of a_{ix}. The coefficients a_{ix}, the constants C_x and their standard deviations which best fit eqn. (19) may be determined from chi-squared minimisation techniques of the whole data set (Press, Flannery, Teukolsky and Vetterling 1986), where

$$\chi^2(x) = \sum_s \left| \frac{\sum_i a_{ix} N_i^s + C_x - N_x^s}{\sigma_s(x)} \right|^2 . \qquad (25)$$

with $\sigma_s(x)$ being the total statistical noise in the analysis of each spectrum s. The variance $\sigma_s^2(x)$ is given by the sum of the variance in the minority atom counts N'^s_x, variance in fitted host counts $a_{ix}^2 N'^s_i$ and variance due to background subtraction. Thus

$$\sigma_s^2(x) = N'^s_x + a_{bx}^2 N_{bx}^s + \sum_i a_{ix}^2 (N'^s_i + a_{bi}^2 N_{bi}^s) \qquad (26)$$

where terms a_{bi} and a_{bx} are scaling constants for host and minority atom background counts, and depend on both window position and width. N'^s_i and N'^s_x are host atom and minority counts prior to background subtraction, with N_{bi}^s and N_{bx}^s the associated background.

Provided the experimental data set S is large so that eqn. (19) is satisfied with a large number of degrees of freedom S', then the reduced chi-squared value

$$\chi_R^2(x) = \frac{\chi^2(x)}{S'} \qquad (27)$$

is expected to be close to unity, and equal to unity if the model given by eqn. (19) is exact. If it is significantly greater than unity, the model is inadequate, and if less than unity, the noise $\sigma_s(x)$ has been incorrectly estimated. Partial failure of the model may be ascribed either to differences in individual X-ray count rate responses with changes in channelling conditions caused by variations in

delocalization or absorption (i.e. the extent to which the assumption that F_{ix}^{s} may be replaced by F_{i}^{s} in eqn. (18) is invalid) or to occupancy of interstitial sites by the additional alloying species (thus negating the constraint that the relative occupancies z_{nx}/z_{ni} should be independent of τ_n).

5. Experimental

Ternary, quaternary and quinternary duplex ($\gamma+\alpha_2$) Ti-Al alloys with ternary compositions $(Ti_{52}Al_{48})_{97}X_{3.0}$ (with x = V, Cr, Ta, Nb), quaternary compositions $(Ti_{52}Al_{48})_{97}X_{1.5}Y_{1.5}$ (with x+y = V+Ta, V+Nb, Cr+Ta, Cr+Nb, Ta+Nb), and quinternary compositions $(Ti_{52}Al_{48})_{97}X_{1.0}Y_{1.0}Z_{1.0}$ (with x+y+z = V+Cr+Nb, V+Ta+Nb, Cr+Ta+Nb) were prepared as 30 g ingots by argon-arc melting on a water cooled copper hearth using a non-consumable tungsten electrode. Each ingot was homogenised by turning and melting five times followed by hot isostatic pressing under argon at 130 MPa for 2 hours at 1573 K. The ingots were then heat treated for 6 hours at 1473 K under argon at atmospheric pressure to establish a γ/α_2 duplex structure. Sections were cut from each ingot by electric discharge machining, mechanically polished and etched for examination by optical microscopy. Electrolytically thinned 3mm diameter disc-specimens of the alloys were mounted in a Gatan cold stage and examined in a Philips CM30 electron microscope at 100 K using 201.5 ± 0.2 keV electrons (this beam energy being determined from positions of HOLZ lines in a <111> Si CBED pattern (Rossouw and Miller, 1993)). A 0.2 μm beam with a 1.8 mrad total convergence angle was aligned along various zone axes of both the γ-phase and α_2-phase, focussed onto a region of the specimen approximately 2000 Å thick and rocked about two orthogonal axes. Beam rocking was externally controlled by computer, with a preset number of pixels in orthogonal angular scan directions and preset acquisition time. The total x-scan range was 190 mrad and y-scan range 140 mrad. Variations in characteristic X-ray emission

as a function of orientation were derived from a full 2048 channel EDX spectrum (stored for each pixel), and displayed as a 79 x 58 pixel X-ray ICP corresponding to a total of S = 4582 results for subsequent statistical analysis. The energy windows were appropriately set for Al and Ti K_α counts, with appropriate windows for characteristic counts from the additional alloying elements x,y and z and for background subtraction. X-ray spectra were acquired at a count rate up to 10^4 counts/sec, with 1-2 sec/pixel over a period of 2 hours. Backscattered electron (BSE) channelling maps were simultaneously recorded, and were used as a guide in setting up experimental conditions prior to allocating control to the computer, since this contrast may be viewed rapidly and is closely related to ICP contrast from X-ray emission (Rossouw 1995).

Initial examination by transmission electron microscopy (TEM) showed that, for the quaternary and quinternary alloys, the widths of the α_2 lamellae were typically less than 0.1μm. It was found that such widths were either smaller than or comparable to the lateral drift of the electron beam that occurs during data collection, and were therefore unsuitable for reliable ALCHEMI analysis. To overcome this problem, all 12 alloys were given a further anneal for 100 h at 1473 K so as to establish lamellae of the α_2-phase with widths appreciably greater than 0.1 μm.

6. Alloy Morphology, Composition and Interphase Partitioning of Additions

The results of optical microscopy, TEM and EDX analysis showed that all 12 alloys were two-phase, for both the 6h and 100h heat treatments at 1473 K, containing both γ and α_2 titanium aluminide phases. The γ-phase was found to have a tetragonal $L1_0$ based crystal structure with composition close to $(Ti_{50}Al_{50})_{97}X_3$ for the ternary alloys, $(Ti_{51.5}Al_{48.5})_{97}X_{1.5}Y_{1.5}$ for the quaternary alloys and

$(Ti_{51}Al_{49})_{97}x_1y_1z_1$ for the quinternary alloys. The α_2-phase was found to have a hexagonal DO_{19} based crystal structure with composition close to $(Ti_{60}Al_{40})_{97}x_3$, $(Ti_{59}Al_{41})_{97}x_{1.5}y_{1.5}$ and $(Ti_{60}Al_{40})_{97}x_1y_1z_1$ for the ternary, quaternary and quinternary alloys respectively. All the alloys were found to exhibit a characteristic duplex microstructure (as illustrated in fig. 2) which, for the 6h anneal at 1473 K, consisted of lamellar grains of fine alternate γ/α_2 lamellae (~ 0.1 μm wide) separated by larger equiaxed γ-grains (≤ 100 μm across) together with a relatively low density of (≤ 2 μm wide) faceted α_2 grains and, for the 100h anneal at 1473K, consisted of a relatively low density of alternate γ/α_2 lamellae (~ 3 μm wide) contained within larger equiaxed γ-grains (≤ 250 μm across) together with faceted α_2 grains (≤ 20 μm wide) . The orientation relationship between the γ and α_2 lamellae was found to be:

$$(111)_\gamma \parallel (0001)_{\alpha 2} \quad \text{and} \quad \langle 1\bar{1}0\rangle_\gamma \parallel \langle 11\bar{2}0\rangle_{\alpha 2}$$

with the lamellae separated by interfaces parallel to $(111)_\gamma \parallel (0001)_{\alpha 2}$ planes.

Although EDX analysis has limited reliability for determination of exact compositions (particularly for elements such as Al where low energy characteristic X-rays are generally quite strongly absorbed within the specimen), it can be applied with greater confidence to measure the relative partitioning of extra alloying elements between the γ and α_2 phases, since such measurements are not critically dependent on the absolute values of relative k-factors (Rossouw, Forwood, Gibson and Miller, 1996b). Absorption was taken into account by converting each characteristic X-ray intensity $I_y(t)$ to a corrected intensity I_y^c, using the crystal thickness t as measured by rocking curves in CBED contrast, the geometric factor R (a tilt of 20° towards the detector with takeoff angle 20° yields R = 1.46) and values for the mean free path λ_y calculated from the MAC30 algorithm of Heinrich (1986). $I_y(t)$ was measured using a highly convergent beam to minimise dynamical effects, with the specimen tilted by 20° towards the X-ray detector. I_y^c was then derived from eqn. (12) as

$$I_y^c = \frac{Rt/\lambda_y}{1-e^{-Rt/\lambda_y}} \; I_y(t) \qquad (28)$$

Measured thicknesses and calculated λ_y values for the various phases given in appendix A, together with relative k-factors and measured intensities.

Results obtained in this way from the 12 different alloys are shown in fig. 3 as the ratio of the alloying element content in the γ-phase to that in the α_2-phase for V, Cr, Ta and Nb in each alloy. It can be seen that, within the limits of experimental error, the partitioning of each individual alloying element is independent of whether the alloy is ternary, quaternary or quinternary. Both V and Cr partition preferentially into the α_2-phase, Ta less strongly so, and Nb shows a slight tendency to favour the γ-phase.

7. Atomic Site Occupancy

7.1. *γ-Phase Analysis*

The total EDX spectrum obtained after completion of the ALCHEMI experiment for the γ-phase of each alloy is shown in fig. 4. All ICPs were recorded from K-shell emissions, except for Ta where the L-shell emissions were used and, since significant peak overlap occurred between Ti K_β and V K_α emissions, the intensity of the V K_β peak was monitored. For the case of V+Cr alloying additions, the V K_β emissions overlap with the Cr K_α, which makes an independent assessment of the V ICP extremely difficult in this situation, although the Cr ICP may be derived from the Cr K_β peak. Appropriate window widths were chosen, together with windows for background subtraction. These widths were typically 33 channels wide for Al and 40 for Ti, V and Cr K-shell excitations, 40

and 70 for Ta L_α and L_β excitations, and 50 for Nb K-shell excitations respectively (the energy range being 10 eV per channel). The results of ALCHEMI analyses for the γ-phase of all 12 alloys are given in Appendix A, and selected examples of ternary, quaternary and quinternary ALCHEMI analyses (for alloying additions of Cr, Cr+Ta, Cr+Nb, and Cr+Ta+Nb respectively) will be shown in full graphical representation, in order to illustrate the type of information contained in a set of experimental data.

A unit cell of the idealised stoichiometric γ-phase $L1_0$ structure (a = 3.986 Å, c/a = 1.02 (Rossouw *et al* 1997)) is illustrated in fig. 5(a), showing both Al sites (at [0 0 0] + n <½ ½ 0]) and Ti sites (at <½ 0 ½] relative to Al). Octahedrally-coordinated sites in fig. 5(b) and tetrahedrally-coordinated interstitial sites in fig. 5(c) are located at ½<100] and ¼<111> respectively from either Al or Ti lattice sites.

Projected structures for different zone axes are shown in figs. 6(a-d), where the edges of the tetragonal cell are shown, with the c-axis projected along the horizontal direction in all cases. Both octahedral and tetrahedral interstitial sites are resolved in projection from substitutional sites for the $[11\bar{2}]$ zone in fig. 6(a). The crystal is tilted about a $[1\bar{1}0]$ vector to a $[11\bar{1}]$ zone in fig. 6(b), where both types of interstitials project equally onto both Al and Ti sites. Further tilt to a [110] zone in fig. 6(c) distinguishes best between both the host atom sites and the two types of interstitial sites. Subsequent tilt about an orthogonal [001] vector accesses the [100] zone in fig. 6(d). Here tetrahedral sites are resolved sites in projection, but octahedral sites project equally onto both Al and Ti atomic strings. In ICPs obtained from these projections, a horizontal $(1\bar{1}0)$ Kikuchi band is common to the first three zones, whilst a vertical (001) band is common to the last two.

ICPs were calculated in terms of dynamical enhancement factors F, using up to 101 beams in the zeroth order Laue zone for an idealised stoichiometric alloy. Elastic scattering potentials were derived from Doyle-Turner parameters (Doyle and Turner 1968), the mean inner potential being 21 volts. $\langle u^2 \rangle$ was taken to be 3.94×10^{-3} Å^2 for Al and 3.86×10^{-3} Å^2 for Ti from the measured Debye-Waller factors at 100 K (Rossouw *et al* 1997), and an Einstein model for thermal absorption was used to calculate mean and anomalous absorption (Allen and Rossouw 1989). A further mean absorptive component (mean free path 2000 Å) was added to account for dechannelling from delocalized electronic excitations. The Al and Ti responses were calculated for a localized thermally-smeared Lorentzian interaction of half-widths b_y = 0.1417 Å and 0.0565 Å for Al and Ti respectively (see Appendix A), and ionization potential of various appropriate widths were used to calculate ICPs for additional alloying atoms, located either on substitutional or interstitial sites (Rossouw *et al* 1996a). The thickness was assumed to be 5000 Å in all cases, and the absorptive mean free paths for characteristic X-rays in the two phases are given in Appendix A. Calculated structure factors for the γ-phase have been published by Rossouw *et al* (1996b). To simulate responses from interstitial sites, a 'test' atom with b = 0.02 Å and an absorptive mean free path of 100 μm for X-ray absorption was used. BSE patterns are closely related to X-ray ICPs, and calculations (Rossouw 1995) were performed for a detector acceptance angles of 132°-157°.

[110] zone

Experimental ICPs for the Cr ternary alloy (alloy 2) and Cr+Ta quaternary alloy (alloy 7) are shown for the [110] zone in fig. 7. Overall enhancement of the Al response occurs between horizontal and vertical 1st and 2nd order BZ boundaries, whereas enhancement of the Ti response occurs between first order boundaries. The enhancement evident between horizontal $(1\bar{1}0)$ and $(2\bar{2}0)$ bands for incoherent scattering from Al correlates well with theory in fig. 8, where a tilt of $\phi = 28°$ was used. Clearly in

alloy 2 of fig. 7, the Cr ICP is most closely correlated with that from Al, and the statistical multivariate fit of the Al and Ti ICPs to that of Cr is shown as the ratio 'Cr/sum'. Calculated tetrahedral and octahedral site ICPs in fig. 8 shows distinctly different contrast from that obtained from Cr in alloy 2 of fig. 7. This result indicates that there is no significant occupancy of interstitial sites by Cr atoms. Similar results were obtained for all 12 alloys, and it was concluded that none of the ternary, quaternary or quinternary alloy additions occupied interstitial sites in the γ-phase. In the case of the quaternary Cr+Ta alloy (alloy 7), fig. 7 shows that, whilst Cr contrast remains closely allied to Al, Ta contrast is very similar to Ti. Note that the BSE ICP in both alloys has elements of Al and Ti contrast characteristics, the contribution of each atom to the BSE contrast being proportional to the atomic number squared (Rossouw, Miller, Josefsson and Allen 1994).

[11$\bar{1}$] zone

Experimental ICPs for the quaternary Cr+Nb alloy (alloy 8) and quinternary Cr+Ta+Nb alloy (alloy 12) are shown in figs. 9 (i) and (ii) near the [11$\bar{1}$] zone. Enhancement of the Al response occurs between horizontal (1$\bar{1}$0) and (2$\bar{2}$0) BZ boundaries, compared to within first order (1$\bar{1}$0) BZ boundaries for the Ti response. An excess cross is formed from angled (202) boundaries, and a hole in the central region of the Al ICP occurs within first order (1$\bar{1}$0) and (101) boundaries. All aspects of these features compare well with computations in fig. 10 for a tilt $\phi = 9°$. It is evident once more that Cr contrast mimics that of Al, whilst both the Ta and Nb contrast closely resembles the Ti ICP. Since tetrahedral and octahedral sites project equally onto both Al and Ti columns, they share the same calculated interstitial site response in fig. 10 which is similar to an incoherent summation of ICPs from Al and Ti sites in fig. 9. This zone is thus inappropriate for distinguishing between substitutional and interstitial site responses.

The full numerical analyses of the ALCHEMI data for each of the 12 alloys is given in Appendix A and is summarised in fig. 11. It can be seen from fig. 11, that atomic site occupancy is influenced by cross-elemental effects. The occupancy of Cr onto Al sites is 69% for the ternary alloy. For the quaternary alloy, occupancy of Cr onto Al sites increases to 77% in the presence of Nb and increases further to 90% in the presence of Ta. For the quinternary alloy, Cr substitutes fully onto Al sites in the presence of both Ta and Nb additions. From fig. 11 it is also evident that V distributes across both Ti and Al sites, slightly favouring Al in the presence of Ta or Ta+Nb additions. More than 80% of Ta occupy Ti sites for all alloys, and more than 90% of Nb occupy Ti sites. The reduced chi-squared results for all analyses are also shown in fig. 11, showing a good fit of experimental data to the model.

It is interesting to note that, within the limits of experimental error, individual ternary additions of V, Cr, Ta and Nb at a concentration of 3 at.% exhibit the same site occupancy as that found previously at a concentration of 1 at.% (c.f. Rossouw *et al* 1996b).

7.2. α_2-*Phase Analysis*

The idealised Ti_3Al α_2-phase with the hexagonal DO_{19} structure is shown in fig. 12, where a = 5.807 Å and c/a = 0.803 with Al atoms located at [0000] and 1/6[20$\bar{2}$3] and Ti atoms at 1/6[$\bar{1}$2$\bar{1}$0], 1/6[2$\bar{1}\bar{1}$0], 1/6[11$\bar{2}$3], 1/6[$\bar{1}$3$\bar{2}$3], 1/6[12$\bar{3}$3] and 1/6[01$\bar{1}$3]. Within this structure, octahedral interstitial sites are located at [0,2,$\bar{2}$,±3]/12, [4,0,$\bar{4}$,±3]/12, [$\bar{2}$,6,$\bar{4}$,±3]/12 and [2,4,$\bar{6}$,±3]/12 with respect to Al sublattice sites, and tetrahedral sites at ±[0,0,0,3]/8 with respect to both Ti and Al lattice sites. It can be seen in the [0001] projection of fig. 13 that good discrimination occurs between Al and Ti sites, whereas in the [11$\bar{2}$0] projection some overlap between Al and Ti sites occurs. In calculating the various ICPs, a $\langle u_s^2 \rangle$ value of 6.33×10^{-3} Å^2 was assumed for all atoms and non-stoichiometry was

accommodated by the excess Al atoms being randomly distributed on available Ti sites, as derived from CBED data (Rossouw *et al* 1996b).

[0001] zone

Experimental ICPs obtained from the [0001] zone are shown in fig. 14 for the quinternary alloy with Cr+Ta+Nb additions. These ICPs have 6-fold rotational symmetry and show a broad weak excess vertical band within the $(40\bar{4}0)$ BZ boundary for both Al and Ti. Away from the zone centre, a horizontal $(\bar{1}2\bar{1}0)$ BZ band is deficit for Al and excess for Ti. Between $(\bar{1}2\bar{1}0)$ and $(\bar{2}4\bar{2}0)$ BZ boundaries, a narrow excess band occurs on Al with a relative decrease on Ti. Differences in detail between Al and Ti occur near the exact zone axis orientation which is evident in the Al/Ti ratio. The Al/Ti ratio is also strongly diminished within $(\bar{1}2\bar{1}0)$ bands, and to a lesser extent within $(20\bar{2}0)$ bands. All these features are in good agreement with the corresponding computed images in fig. 15 where the tilt $\phi = 15°$. The noisy experimental ICPs from Cr, Ta and Nb do not at first offer a clear indication of which site the addition occupies. However, numerical ALCHEMI analysis returns values for site occupancy as 44±5 % for Cr onto Al sites, and 84±7 % for Ta and 82±8% for Nb onto Ti sites.

The sensitivity of the [0001] zone axis to the occupation of interstitial sites by the ternary additions is illustrated in the calculated ICPs of fig. 15. For the tetrahedral interstitial site, the computed ICP displays features similar to that of a summation of Al and Ti responses, whereas the computed ICP for the octahedral site has deficit $(40\bar{4}0)$ bands but excess $(\bar{2}4\bar{2}0)$ bands. Experimental ICPs from the additional alloying elements show no correlation with the calculated octahedral site response, indicating that there is no significant occupancy of octahedral interstitial sites by the ternary atoms. However, for this projection, comparisons of experimental and calculated ICPs do not allow conclusions to be drawn concerning the occupation of tetrahedral interstitial sites.

[$\bar{1}\bar{1}$23] zone

Figure 16 demonstrates the type of ICP contrast obtained using the [$\bar{1}\bar{1}$23] zone axis. The computed ICPs show differences between Al and Ti responses near the centre of the zone, with a decrease occurring near the centre of the ICP for Al where Ti has a strong maximum. Strong enhanced lobes for Al occur within the horizontal (11$\bar{2}$2) BZ and between the vertical ($\bar{1}$100) and ($\bar{2}$200) BZ boundaries. All these features of contrast correlate well with the calculated patterns fig. 17. The ICPs from Cr and Ta appear to have no correlation with the calculated tetrahedral or octahedral interstitial contrast, indicating that neither type of interstitial site in the α_2-phase is significantly occupied by these alloying additions. As in the case of the γ-phase, this result was found for all 12 alloys, indicating that none of the alloying additions occupy interstitial sites in the α_2-phase. ALCHEMI analysis of the data in fig. 16 indicates that 83±8% of Cr partitions onto Ti sites compared with 86±4% of Ta.

The full numerical ALCHEMI analyses for all 12 alloys are given in Appendix A and is summarised in fig. 18. No HOLZ beams of the α_2-phase were able to be excited with 50-300 keV electrons, presumably since the composition is off-stoichiometry for the idealised $D0_{19}$ structure, leaving a large amount of residual strain, which serves effectively as a temperature-independent contribution to the Debye-Waller factor. The ideal structure would be represented by 25% (atomic percent) Al, however the composition is roughly 60% Ti and 40 % Al. It is assumed that the excess Al atoms are accommodated substitutionally on the Ti sublattice sites, and the matrix has a relatively large degree of compositionally-induced disorder. Thus this structure is not ideal for ALCHEMI experiments. Nevertheless, the results obtained are valid but have standard deviations about 2-4 times greater than those for the γ-phase. Given the large standard deviations involved, the overlap of results for site occupancy as shown in fig. 18 means that most additional atoms appear to have an occupancy of 70-90% onto Ti sites, the solitary exception being Cr in the quinternary alloy Cr+Ta+Nb, where Cr

partitions 56±6% onto Ti sites. It should be noted that large standard deviations occur for analyses involving the V K_β peak.

As for the γ-phase, within the limits of the large experimental errors incurred in the analysis of the α_2-phase, individual ternary additions of V, Cr, Ta and Nb at a concentration of 3 at.% exhibit the same site occupancy as that found previously at a concentration of 1 at.% (c.f. Rossouw *et al* 1996b).

8. Atomic Order

Since no HOLZ beams could be obtained in CBED patterns from the α_2-phase, atomic order could only be investigated in the γ-phase.

8.1. *HOLZ Analysis of γ-Phase*

Figure 19 shows experimental [110] n = 2 HOLZ reflections for the ternary alloy with Ta, the quaternary alloy Cr+Nb and quinternary alloy Cr+Ta+Nb. Three distinct rings are visible. Calculations have indicated that, although the position of the third (outer ring) is relatively insensitive to order, the first (inner) and second (middle) rings come together as the order parameter P decreases and merge completely when P = 0.

Spatial distributions of the Bloch wavefunctions $\phi^{(i)}(\mathbf{r})$ associated with each ring are shown in fig. 20, and can be compared with projected atomic structures in fig. 6. The first (inner) ring is associated with excitation of state (1), with a maximum peaked on Ti sites. The second (middle) ring is

associated with state (2), its maximum being on Al sites. The relatively bright third (outer) ring is associated with Bloch state (5), being negative in open channels between atom sites to a peak of 1.3 on both Al and Ti sites. These three quantum states account for 97.4% of the overall dynamic intensity at the symmetrical zone axis orientation.

The order parameter P may be determined from direct measurements of quantum state HOLZ ring positions. Differences in HOLZ ring positions are associated with different potential energies of the three excited states in the alloys. For example, a fully ordered alloy will have maximum separation in potential energy between states (1) and (2), the potential energy of state (5) being relatively insensitive to ordering. With increasing disorder, the potential energy of state (1) will increase, with a concomitant decrease for state (2). This will result in an outward shift of line (1) from the centre of the pattern, whilst line (2) shifts inward towards the centre of the pattern. For the limit of fully disordered alloy, states (1) and (2) will merge. The different potential energies and absorption of the three excited states in these alloys is determined by the overlap between the respective quantum states $\phi^{(i)}(r)$ of fig. 20(a) and the elastic and TDS absorptive potentials of fig. 20(b).

If the separation in the rocking curve between states (i) and (j) is defined as Δ_{ij}, then the ratio $\Delta_R = \Delta_{12}/\Delta_{15}$ yields a direct measure of order. The measured value of Δ_R for the γ-phase of the binary Ti-Al alloy is 0.495 which a comparison with calculated values indicates a fully ordered state with P = 1.0. The measured values for Δ_R are shown in fig. 21 for the 12 alloys and these values span either side of the result for the fully ordered binary Ti-Al alloy (experimental errors being typically ±10%). This does mean that the state of order is changing between the different alloys, but rather that the separation Δ_{12} is altered by the extent to which a higher atomic number atom occupies a Ti sub-lattice site.

The relative positions of quantum state 'rings' in HOLZ beams have already been shown by Peng and Gjønnes (1989) to be determined by the potential energies of different Bloch states. For the case of γ-phase TiAl and the various alloys, relative positions of quantum HOLZ rings provide a direct 'spectral' method for determining order parameter. This measurement is virtually independent of Debye-Waller factors since, although the *intensity* of each spectral line is extremely sensitive to Debye-Waller factor (Rossouw and Hampikian 1993), the *positions* of quantum states lines are not (Rossouw and Miller 1993). This method has a distinct advantage over less direct refinement procedures, where an assessment of order parameter requires comparisons of intensities between experiment and theory.

9. Conclusions

- The partitioning of each individual alloying element between the γ and α_2 phases is independent of whether it is present as a ternary, quaternary or quinternary addition.
- There is no significant occupancy of interstitial sites by any of the added ternary, quaternary or quinternary alloying elements for both the γ or α_2 phases.
- Within the limits of experimental error, individual ternary additions of V, Cr, Ta and Nb at a concentration of 3 at.% exhibit the same site occupancy as that found previously at a concentration of 1 at.%.
- Two significant examples of cross-elemental effects on atomic site occupancy were found in the γ-phase:

  (i) the site occupancy of Cr on Al sites increased from 69% in the ternary alloy to 77% in the Cr+Nb alloy to 90% in the Cr+Ta alloy to 100% in the Cr+Ta+Nb alloy; indicating that the presence of Nb has little effect on the site occupancy of Cr whereas Ta causes an increased affinity for Al sites and the presence of Ta and Nb in combination causes Cr to completely favour Al sites.

  (ii) ternary additions of V approximately occupy Al and Ti sites equally but in the presence of Ta in both quaternary and quinternary alloys the V atoms strongly favour Al sites.

- Due to the large experimental error incurred in obtaining site occupancies in the α_2-phase the only significant result is that all alloying additions tend to favour Ti sites, except for Cr when it is in the combined presence of Ta and Nb, where it is approximately equally distributed between Al and Ti sites.
- Analysis of rocking curve intensity maxima in HOLZ CBED patterns shows, to an accuracy of ±10%, that all the ternary, quaternary and quinternary alloys are fully ordered with excess Al atoms occupying antisite positions on available Ti sites.

References

Allen, L.J. and Rossouw, C.J., 1989, Phys. Rev. B, **39**, 8313.

Allen, L.J., and Rossouw, C.J., 1993a, Ultramicroscopy, **47**, 2446.

Allen, L.J., and Rossouw, C.J., 1993b, Ultramicroscopy, **48**, 341.

Appel, F., Beaven, P.A., and Wagner, R., 1993, Acta metall. mater., **41**, 1721.

Bird, D.M., and King, Q.A., 1990, Acta Cryst., **A46**, 202.

Cherns, D., Howie, A., and Jacobs, M.H., 1973, Z. Naturforsch., **28a**, 565.

Doi, H., Hashimoto, K., Kasahara, K., and Tsujimto, T., 1990, Mater. Trans. JIM, **31**, 975.

Doyle, P.A., and Turner, P.S., 1968, Acta Cryst., **A24**, 390.

Goldstein, J.I., Costley, J.L., Lorimer, G.W., and Reed, S.J.B., 1977, Scanning Electron Microscopy (1977), edited by O. Johari (IITR:Chicago), pp 315-324.

Hanamura, T., Uemori, R., and Tanino, M., 1988, J. Mater. Res., **3**, 656.

Heinrich, K.F.J., 1986, 11th International Congress on X-ray Optics and Microanalysis, Ed. J.D.Brown and R.H.Packwood, London, Ontario, 67-72.

Horita, Z., Sano, T., and Nemoto, M., 1991, Ultramicroscopy, **35**, 27.

Hou, D.H., Jones, I.P., and Frase, H.L., 1996, Phil. Mag., **A74**, 741.

Huang, S.C., and Hall, E.L., 1991a, Acta metall. mater., **39**, 1053.

Huang, S.C., and Hall, E.L., 1991b, Metall. Trans., **22A**, 2619.

Josefsson, T.W., Allen, L.J., Miller, P.R., and Rossouw, C.J., 1994, Phys. Rev. B, **50**, 6673.

Kim, Y-W., 1989, JOM., **41**, 24.

Kim, Y-W., 1994, JOM., **46**, 30.

Kim, Y-W., and Dimiduk, D.M., 1991, JOM., **43**, 40.

Konitzer, D.G., Jones, I.P., and Fraser, H.L., 1986, Scripta Metallurgica, **20**, 265.

Krishnan, K.M., 1988, Ultramicroscopy, **24**, 125.

Lewis, A.L., Villagrana, R.E., and Metherell, A.J.F., 1978, Acta Cryst., **A34**, 138.

Maslen, V.M., and Rossouw, C.J., 1984, Phil. Mag. A, **49**, 735.

M^{c}Kee, D.W., and Huang, S.C., 1992, Corrosion Science, **33**, 1899.

Mohandas, E., and Beaven, P.A., 1991, Scripta metall. mater., **25**, 2023.

Morinaga, M., Saito, J., Yukawa, N., and Adachi, H., 1990, Acta metall. mater., **38,** 25.

Nuchter, W., and Siegle, W., 1995, Phil. Mag. A, **71**, 165.

Peng, L-M., and Gjonnes, J.K., 1989, Acta Cryst., **A45**, 699.

Pennycook, S.J., 1988, Ultramicroscopy, **26**, 239.

Pennycook, S.J., and Narayan, J., 1985, Phys. Rev. Lett., **54**, 1543.

Press, W.H., Flannery, B.P., Teukolsky S.A., and Vetterling, W.T., 1986, Numerical Recipes (Cambridge University Press), Ch. 14, pp. 498-546

Radi, G., 1970, Acta Cryst., **A26**, 41.

Rossouw, C.J., 1985, Ultramicroscopy, **16**, 241.

Rossouw, C.J., 1995, Ultramicroscopy, **58**, 211.

Rossouw, C.J., and Maslen, V.W., 1984, Phil. Mag. A, **49**, 743.

Rossouw, C.J., Turner, P.S., White, T.J., and O'Connor, A.J., 1989, Phil. Mag. Lett., **60**, 225.

Rossouw, C.J., and Hampikian, J.M., 1993, Phil. Mag. A, **67**, 849.

Rossouw, C.J., Miller, P.R., 1993, Phil. Mag. B, **67**, 733.

Rossouw, C.J., Miller, P.R., Josefsson, T.W., and Allen, L.J., 1994, Phil. Mag. A, **70**, 985.

Rossouw, C.J., Gibson, M.A., and Forwood, C.T., 1996, Phil. Mag. A, **73**, 187.

Rossouw, C.J., Forwood, C.T., Gibson, M.A., and Miller, P.R., 1996a, Phil. Mag. A, **74**, 57.

Rossouw, C.J., Forwood, C.T., Gibson, M.A., and Miller, P.R., 1996b, Phil. Mag. A, **74**, 77.

Rossouw, C.J., Gibson, M.A., and Forwood, C.T., 1997, Ultramicroscopy (in press).

Shindo, D., Hirabayashi, M., Kawabata, T., and Kikuchi, M., 1986, J. Electron Microscopy, **35**, 409.

Smythe, J.R., and McCormick, T.C., 1988, Ultramicroscopy, **26**, 77.

Spence, J.C.H., Kuwabara, M., and Kim, Y., 1988, Ultramicroscopy, **26**, 103.

Spence, J.C.H., and Tafto, J., 1983, J. Microscopy, **130**, 147.

Taftø, J, and Spence, J.C.H., 1982, Ultramicroscopy, **9**, 243.

Turner, P.S., White, T.J., O'Connor, A.J., and Rossouw, C.J., 1991, J. Microscopy, **162**, 369.

Xu, J-H., and Freeman, A.J., 1994, J. Mater. Res., **9**, 1755.

Wunderlich, W., Kremser, Th., and Frommeyer, G., 1993, Acta metall. mater., **41**, 1791.

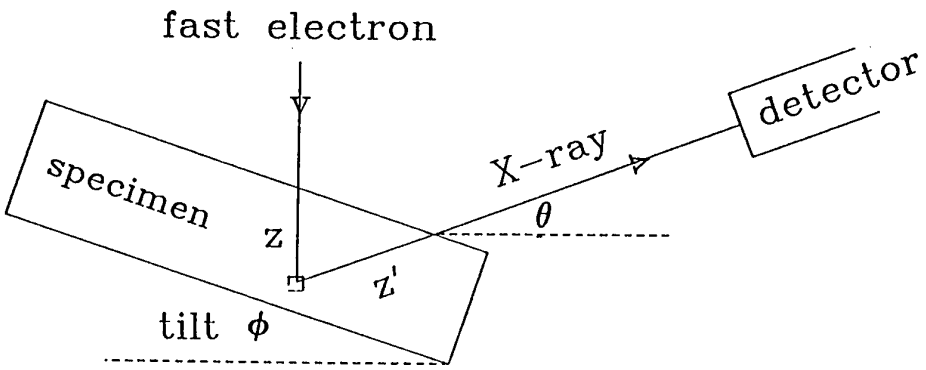

Fig. 1. Schematic diagram of X-rays generated at depth z in a specimen tilted through an angle ϕ towards the detector, traversing a distance z' on their way to the X-ray detector with takeoff angle θ.

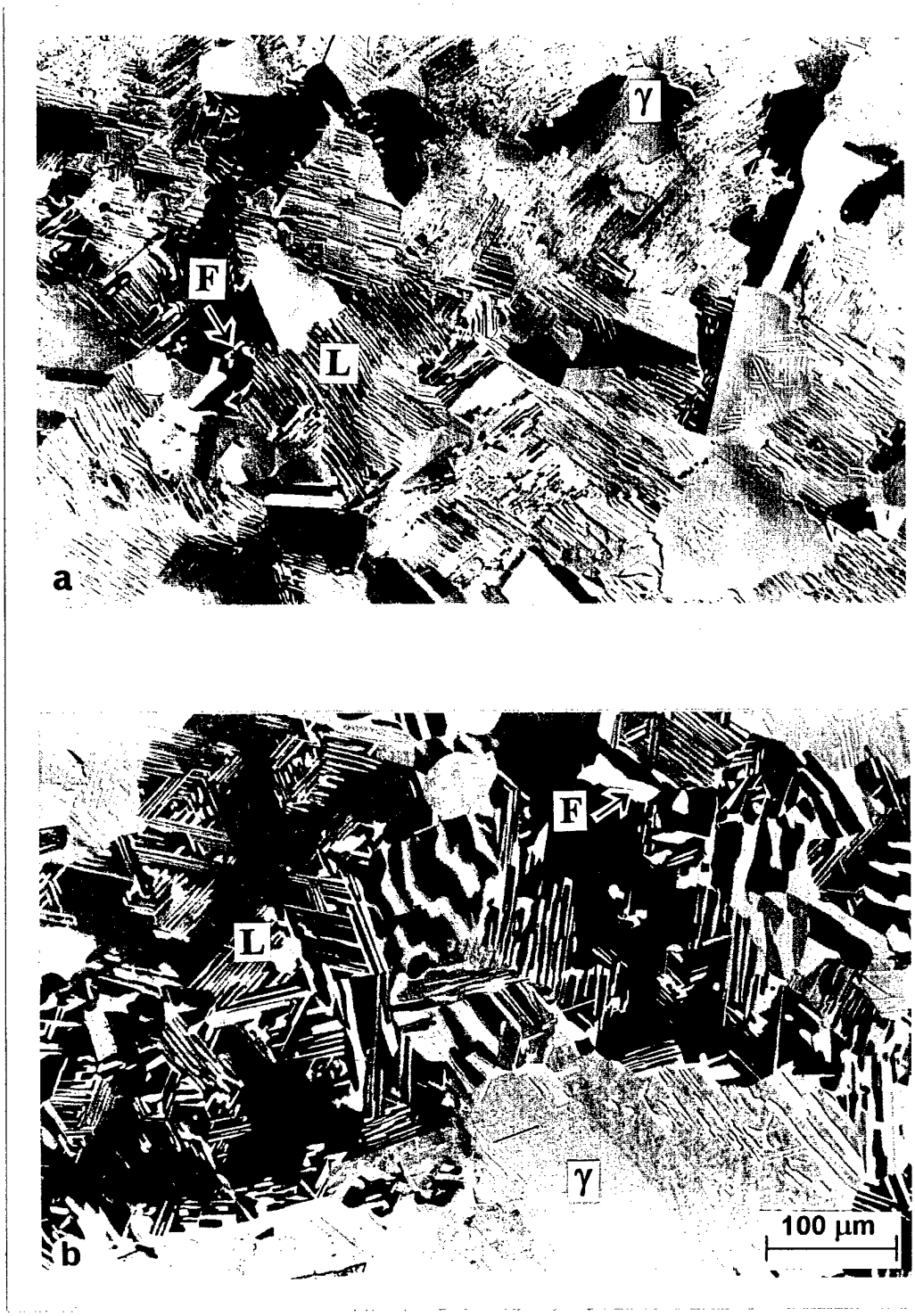

Fig. 2. Optical micrographs of $(Ti_{52}Al_{48})_{97}V_{1.5}Nb_{1.5}$ showing typical duplex microstructure of the alloys used, after annealing at 1473 K for 6h (a) and for 100h (b). Examples of a γ/α_2 lamellae, an equiaxed γ grain and a faceted α_2 grain are labelled L, γ and F respectively.

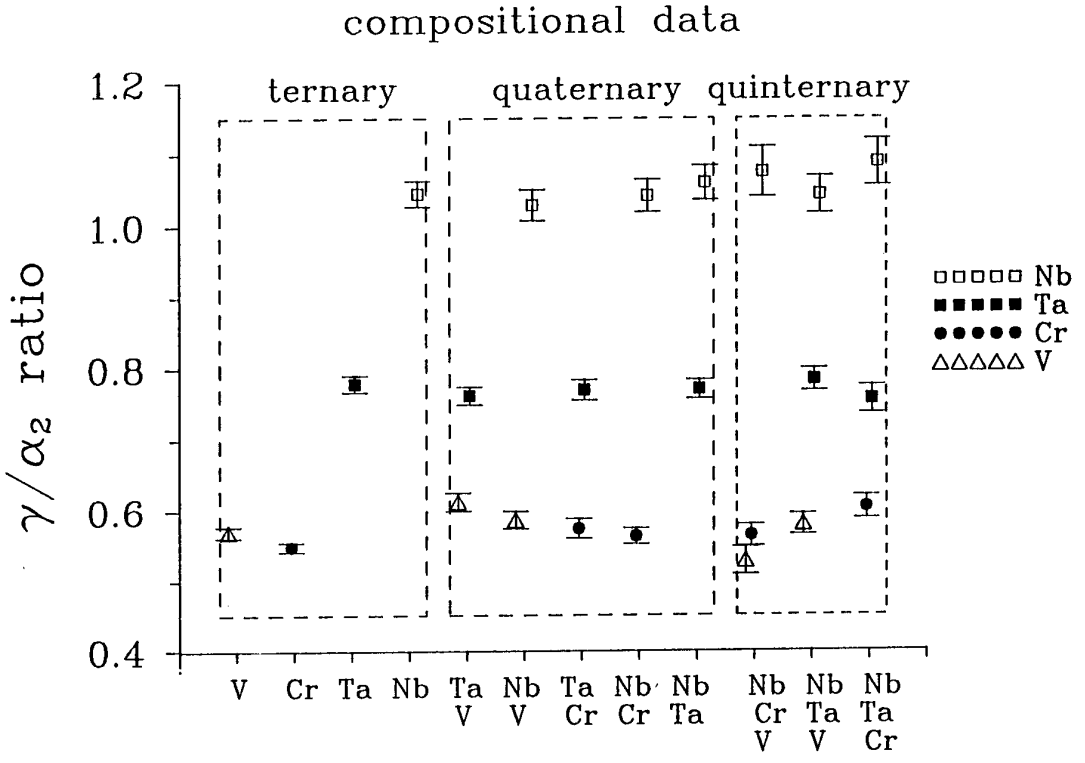

Fig. 3. Composition ratio of ternary, quaternary and quinternary alloying elements in the γ-phase compared with the α_2-phase.

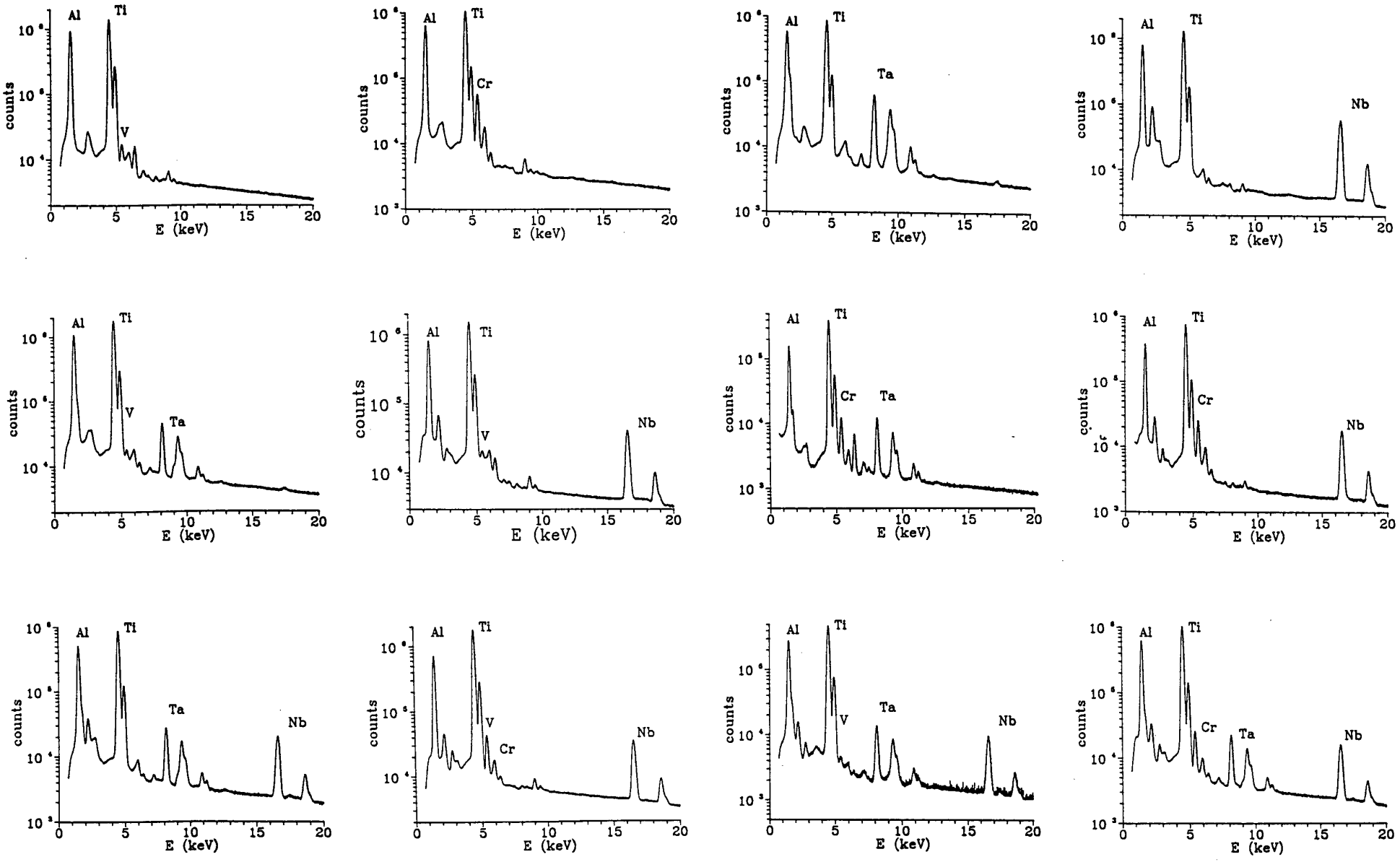

Fig. 4. Total EDX spectra obtained from the γ-phase after completion of the ALCHEMI experiments for all 12 alloys.

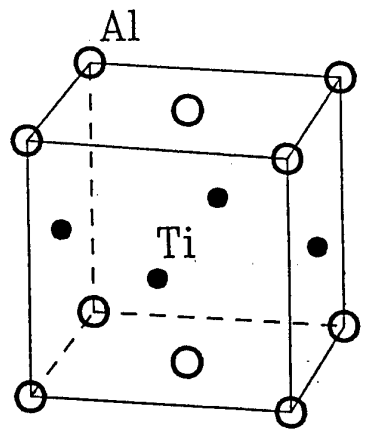

(a)

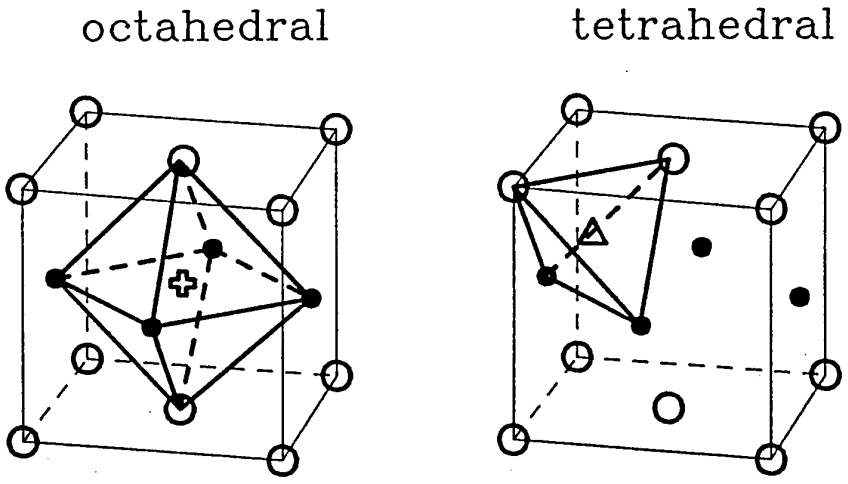

(b) (c)

Fig. 5. (a) $L1_0$ structure for γ-phase TiAl (large open circles, Al; small full circles, Ti) with (b) octahedral and (c) tetrahedral interstitial sites.

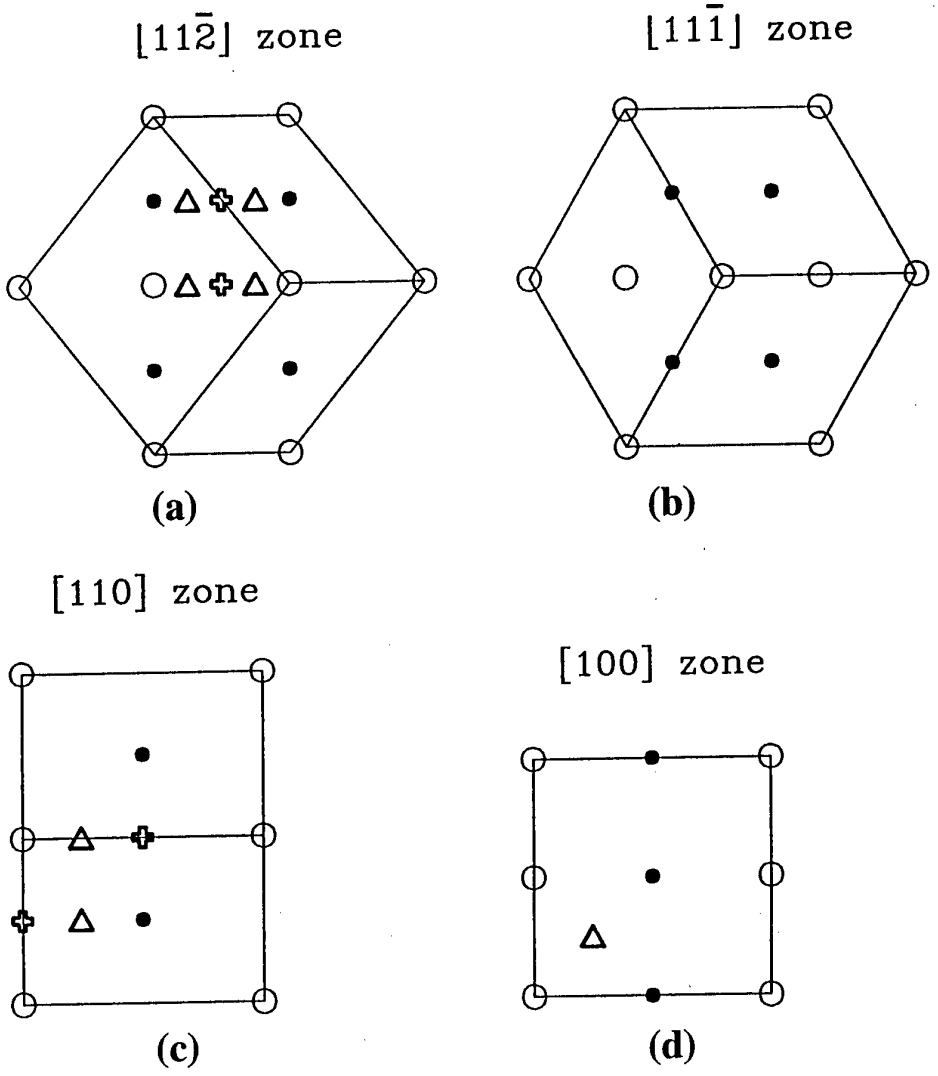

Fig. 6. Projected atomic structures (Al large open circles, Ti small filled circles) of γ-phase for the following zone axes: (a) [11$\bar{2}$] (b) [11$\bar{1}$] (c) [110] and (d) [100]. The vertical lattice vector is [$\bar{1}$10] for (a-c), and [010] for (d). Open triangles indicate tetrahedral interstitial sites, open crosses indicate octahedral sites.

Alloy 2 gamma phase Cr

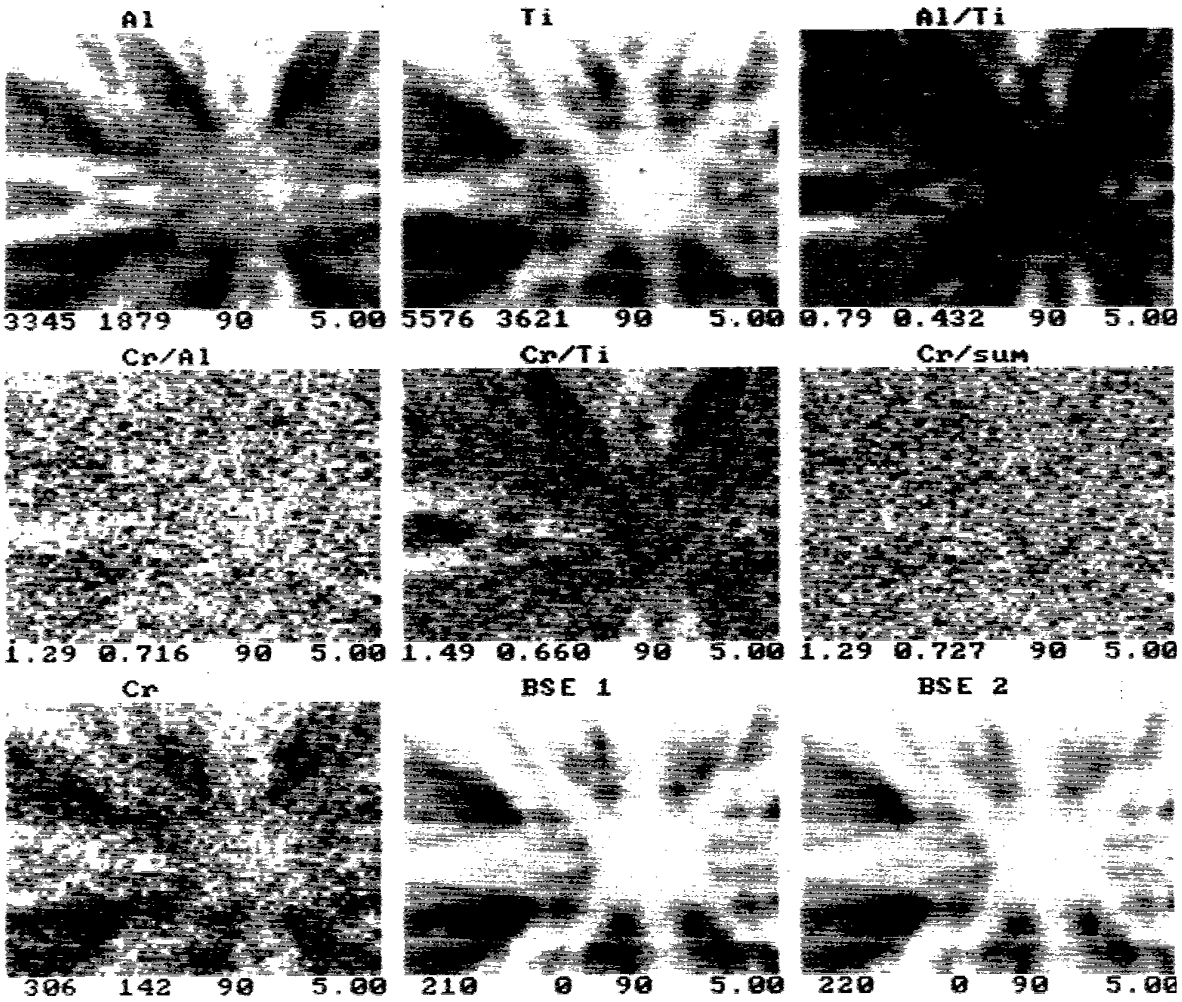

Fig. 7. ICPs obtained from the [110] zone axis of the γ-phase of the Cr ternary alloy (alloy 2) and the Cr+Ta quaternary alloy (alloy 7).

Alloy 7 gamma phase Cr + Ta

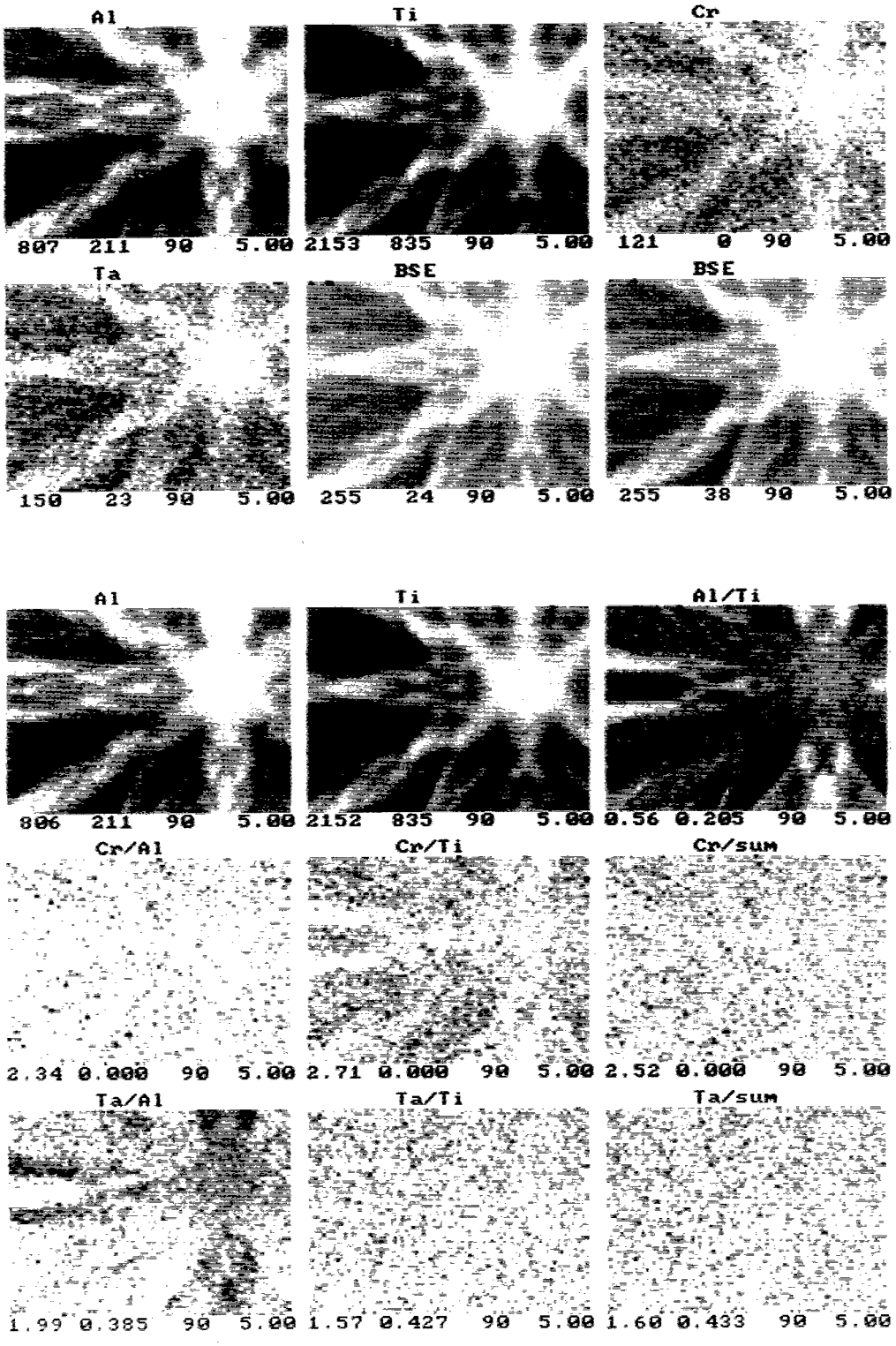

Fig. 7. Continued.

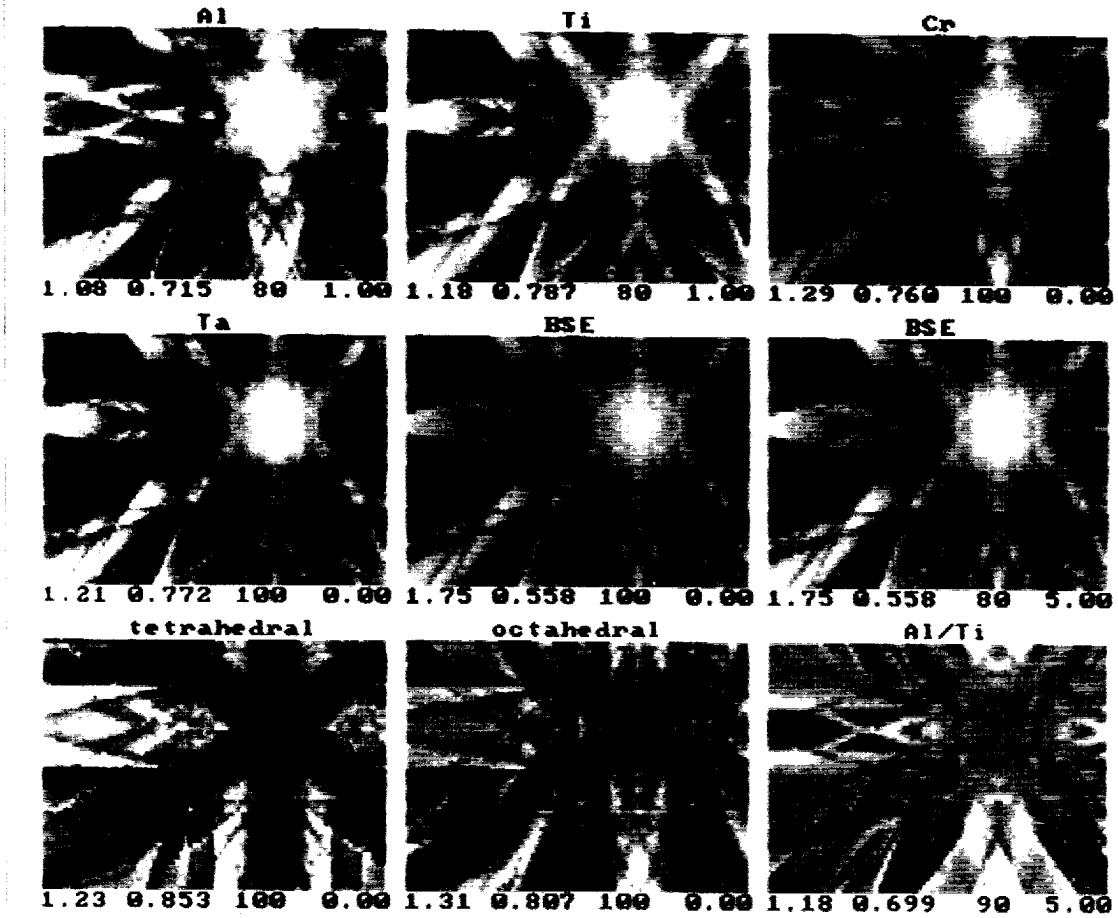

Fig. 8. Calculated [110] ICPs for the γ-phase of the Cr+Ta quaternary alloy, tilt $\phi = 28^{o}$.

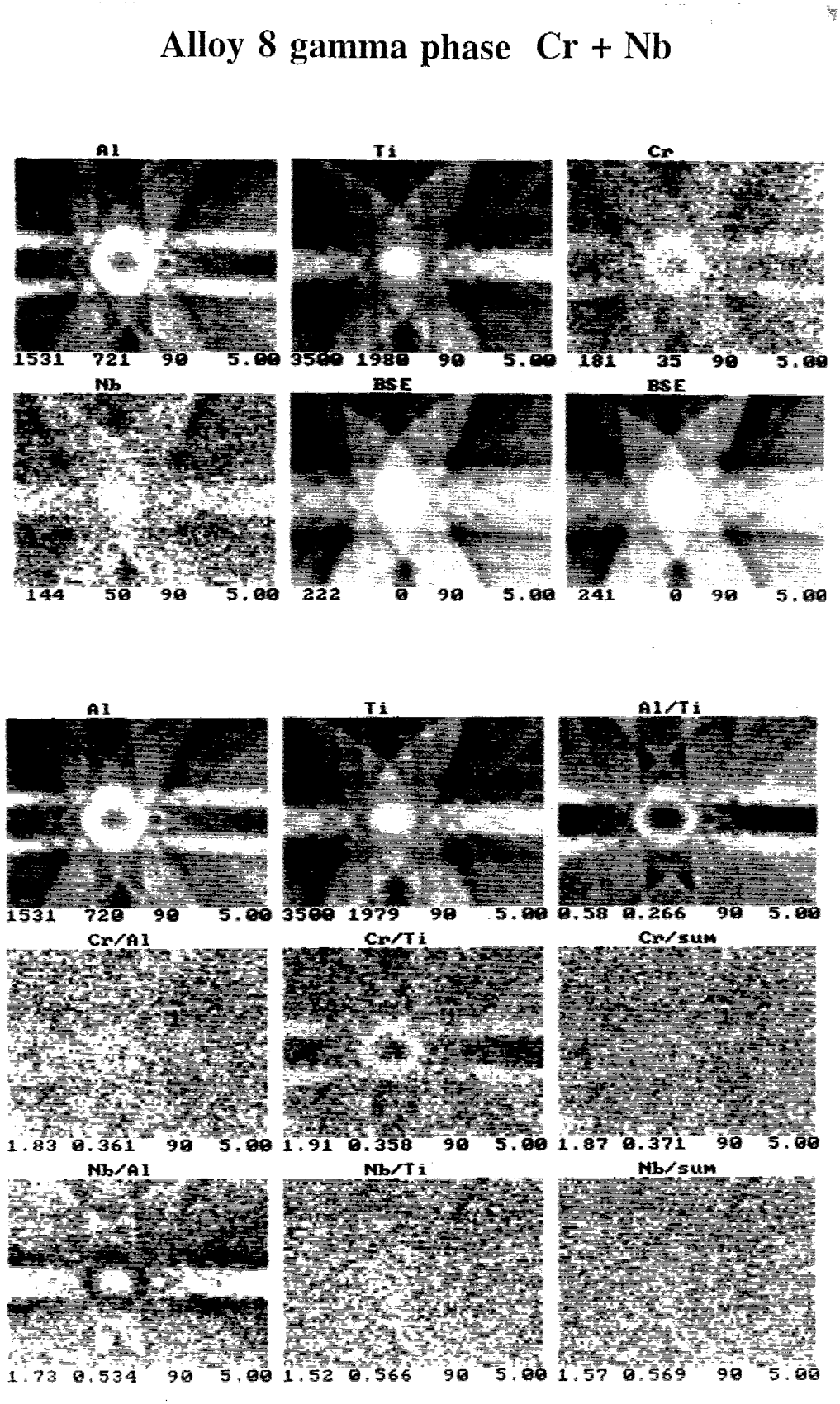

Fig. 9. ICPs obtained from the [111] zone axis of the γ-phase of the Cr+Nb quaternary alloy (alloy 8) and the Cr+Ta+Nb quinternary alloy (alloy 12).

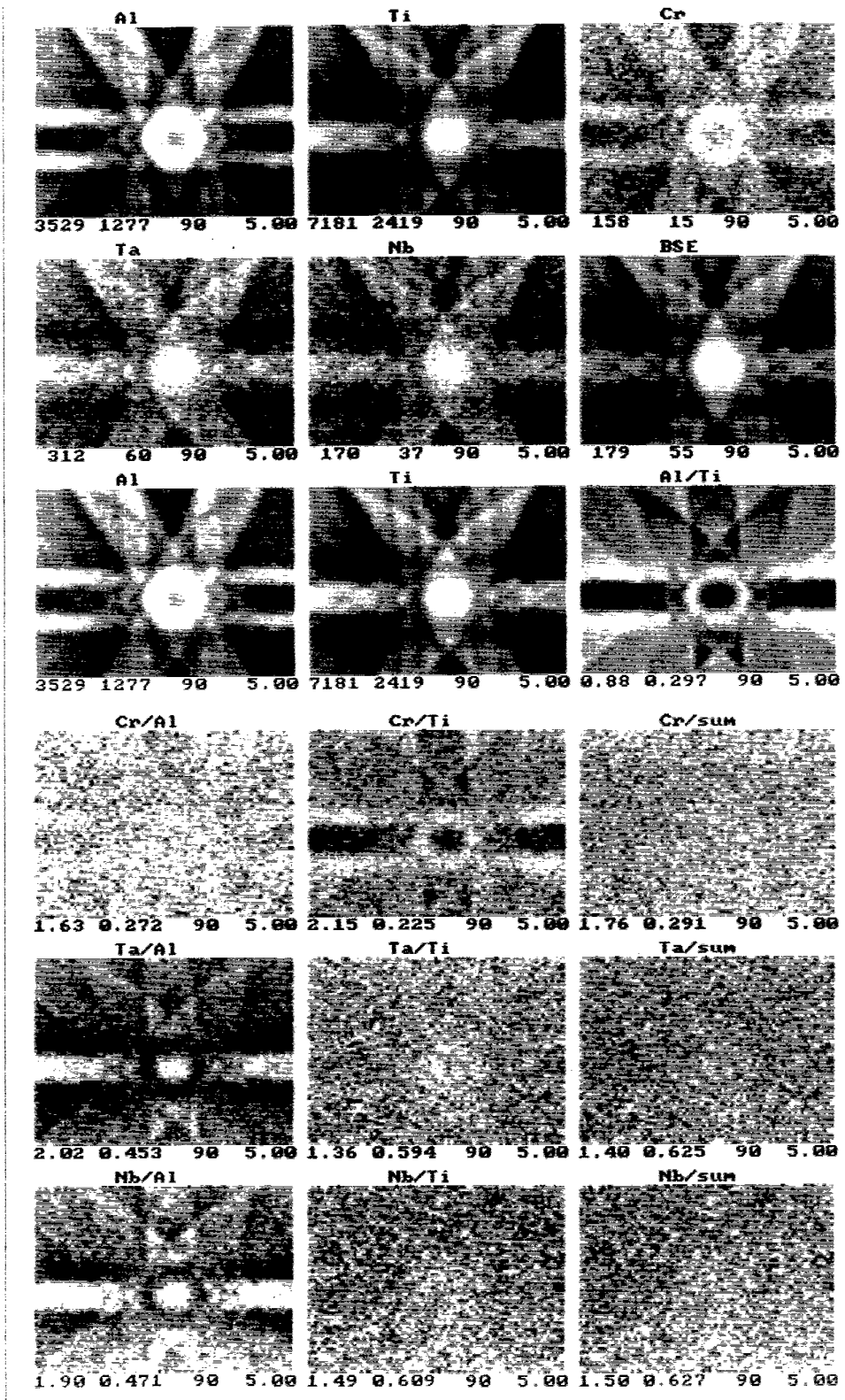

Fig. 9. Continued.

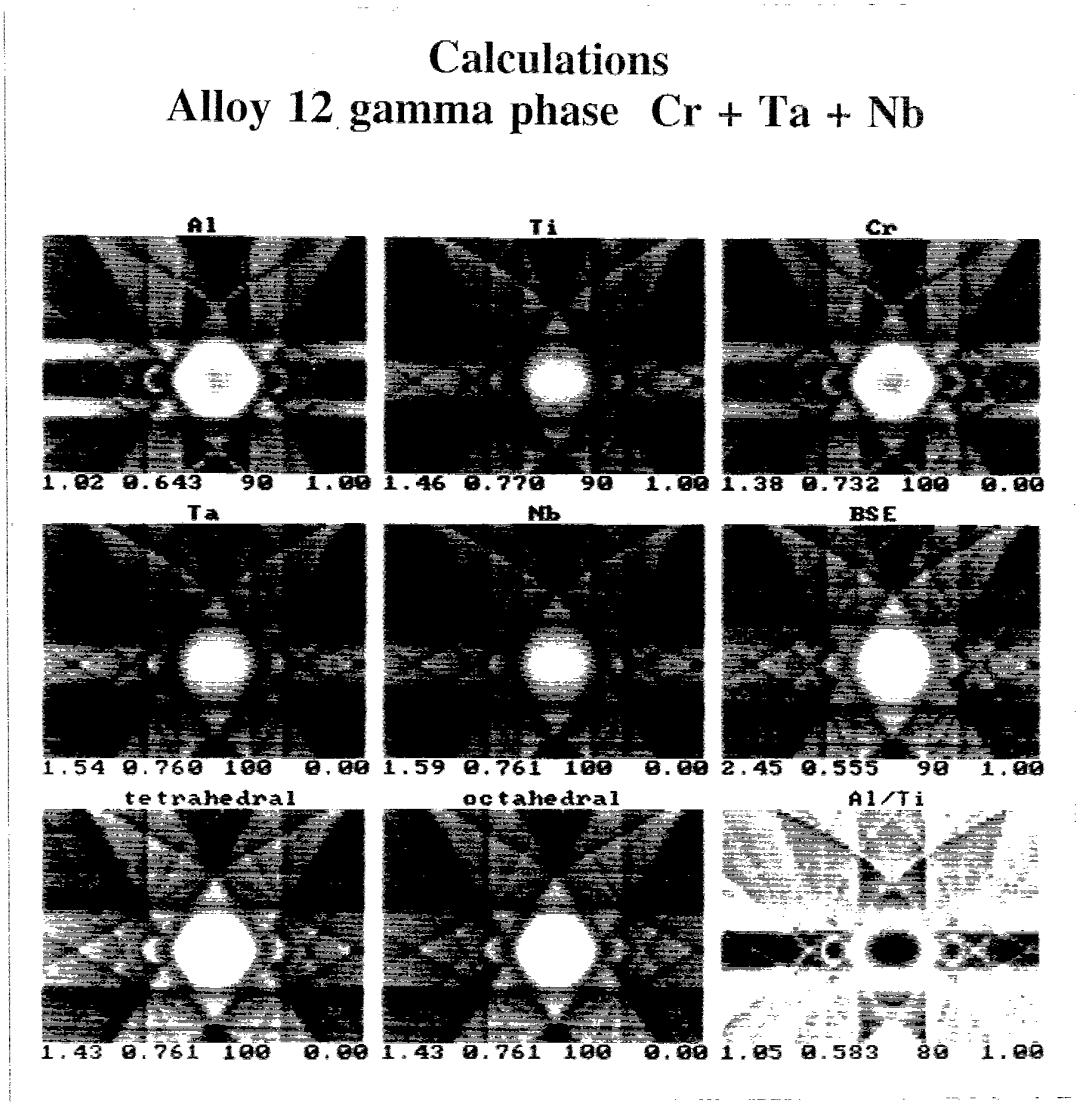

Fig.10. Calculated [111] ICPs for the γ-phase of the Cr+Ta+Nb quinternary alloy, tilt $\phi = 9^{o}$.

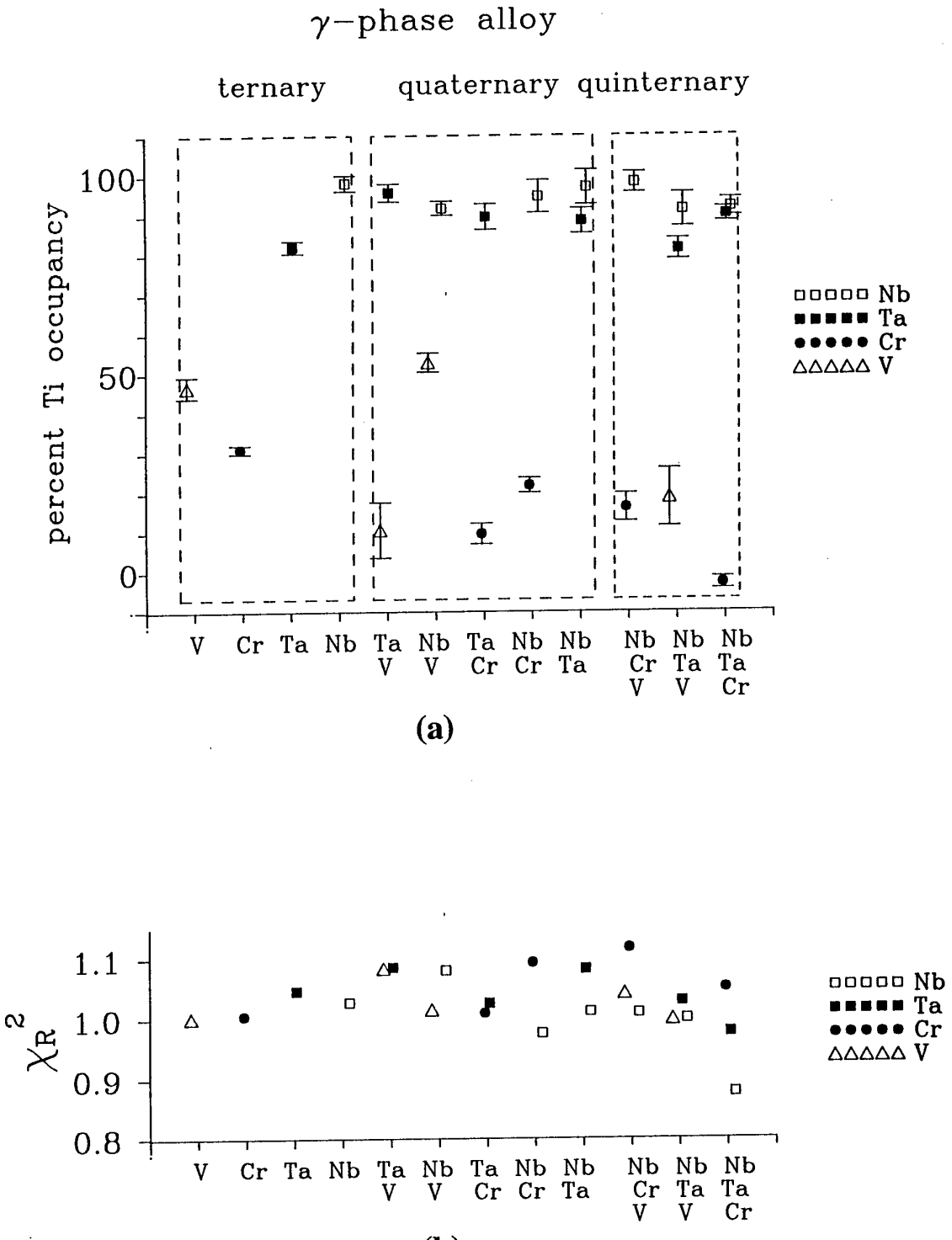

Fig.11. (a) Distribution of ternary, quaternary and quinternary alloying atoms on Ti sites in the γ-phase (error bars indicate one standard deviation) and (b) χ_R^2 obtained from analyses.

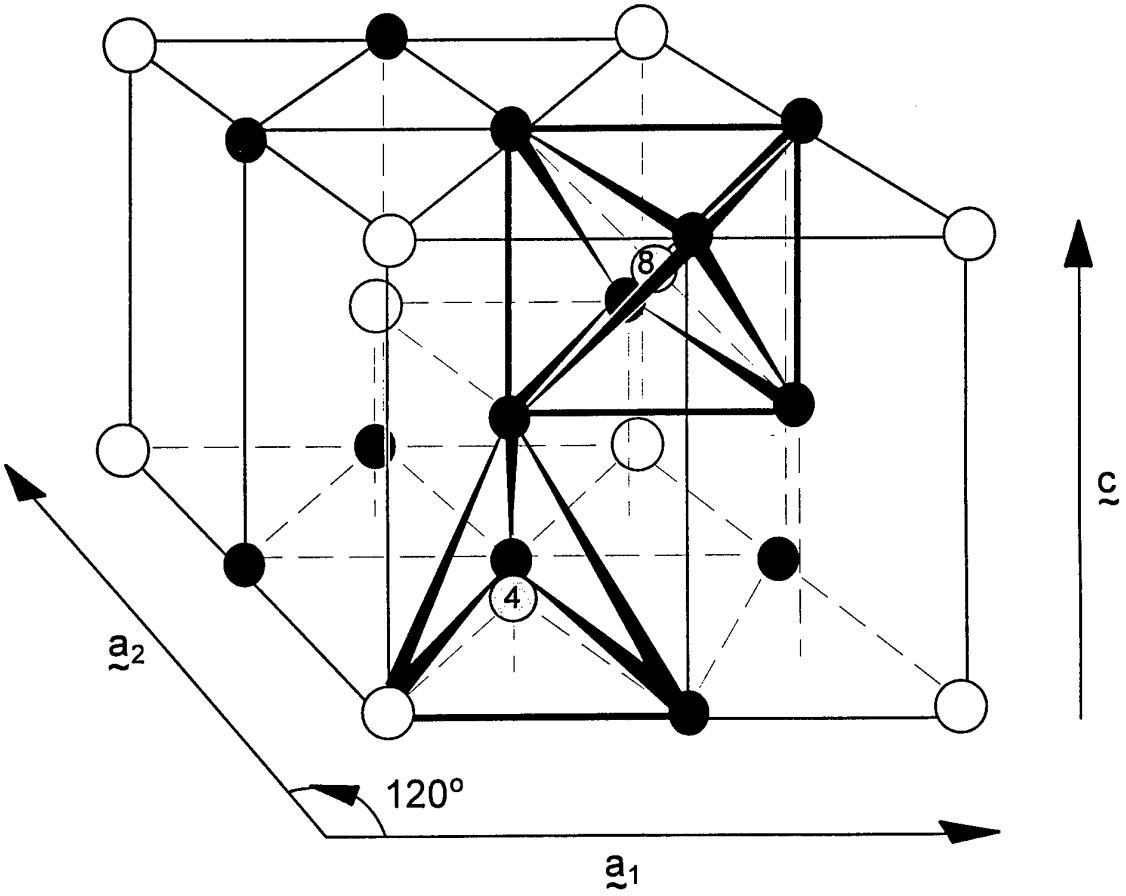

Fig.12. DO_{19} structure for α_2-phase Ti_3Al (large open circles, Al; small full circles, Ti) with octahedral and tetrahedral interstitial sites labelled 8 and 4 respectively.

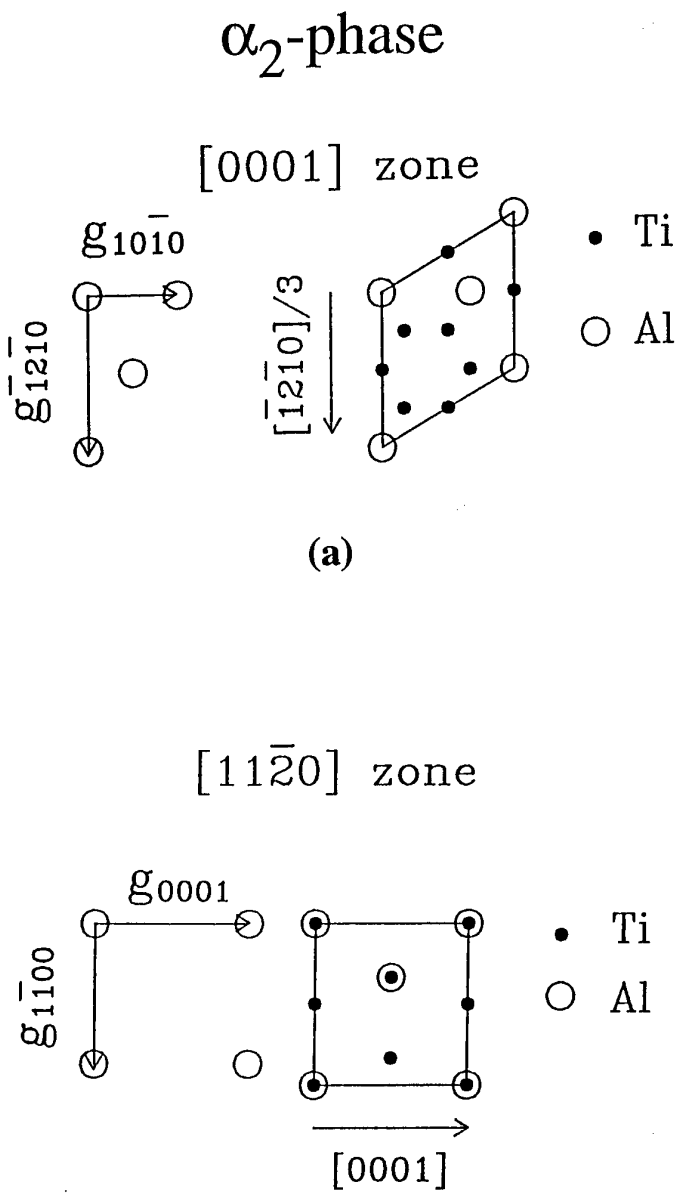

Fig.13. Projected atomic structure of α_2-phase (a) along [0001] zone axis, (b) along $[11\bar{2}0]$ zone axis, (Al large open circles, Ti small full circles).

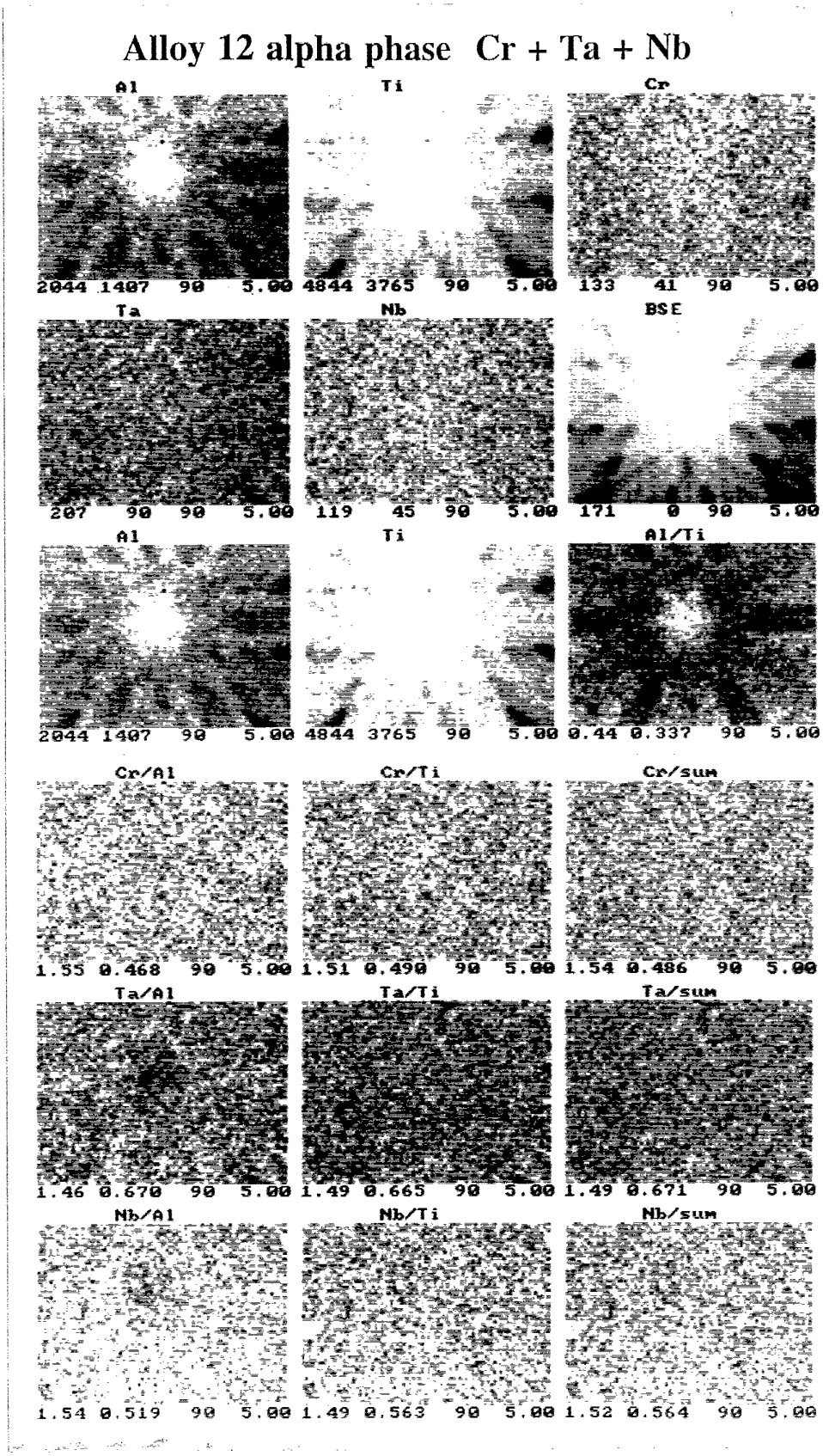

Fig.14. ICPs obtained from the [0001] zone axis of the α_2-phase of the Cr+Ta+Nb quinternary alloy (alloy 12).

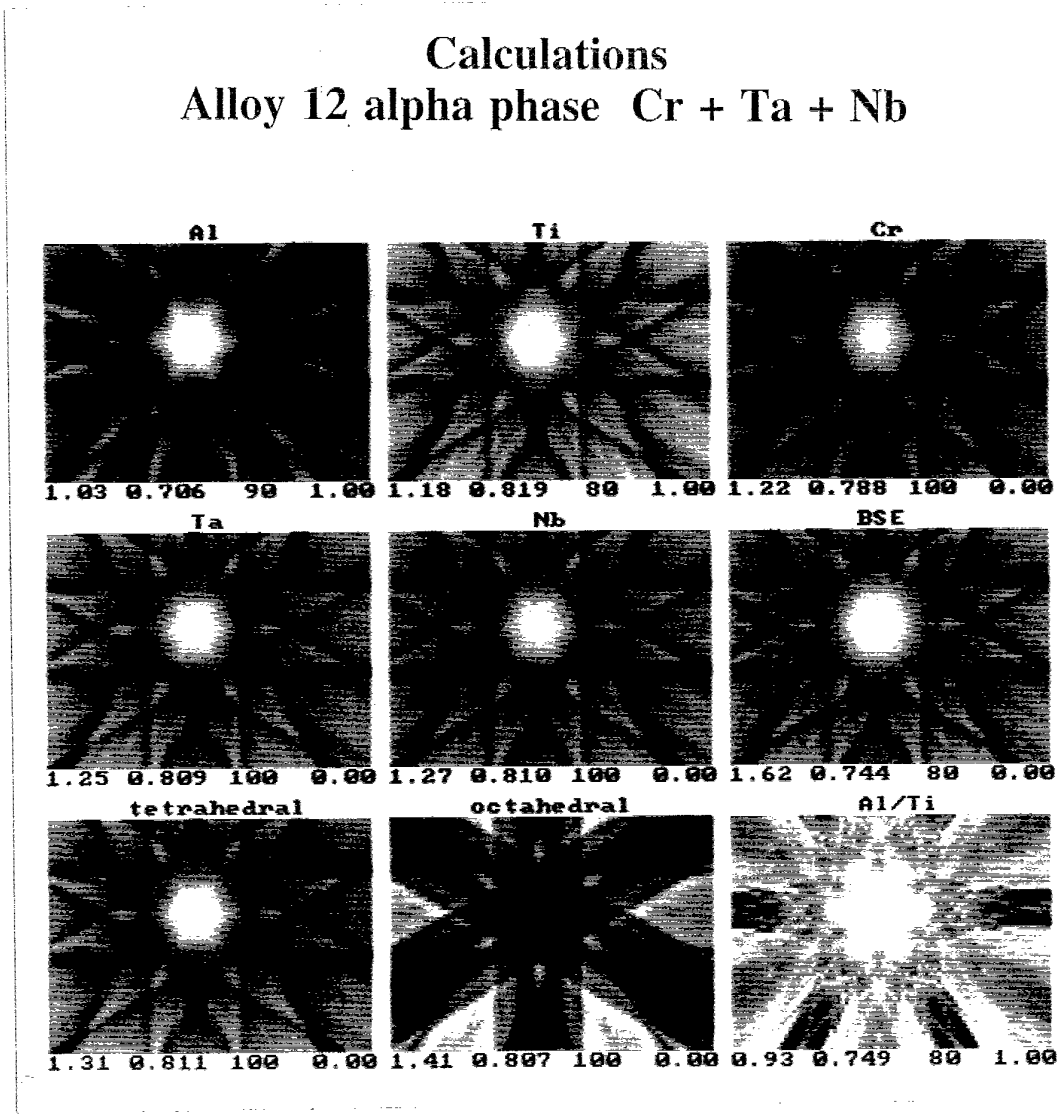

Fig.15. Calculated [0001] ICPs for the α_2-phase of the Cr+Ta+Nb quinternary alloy, tilt $\phi = 18^{o}$.

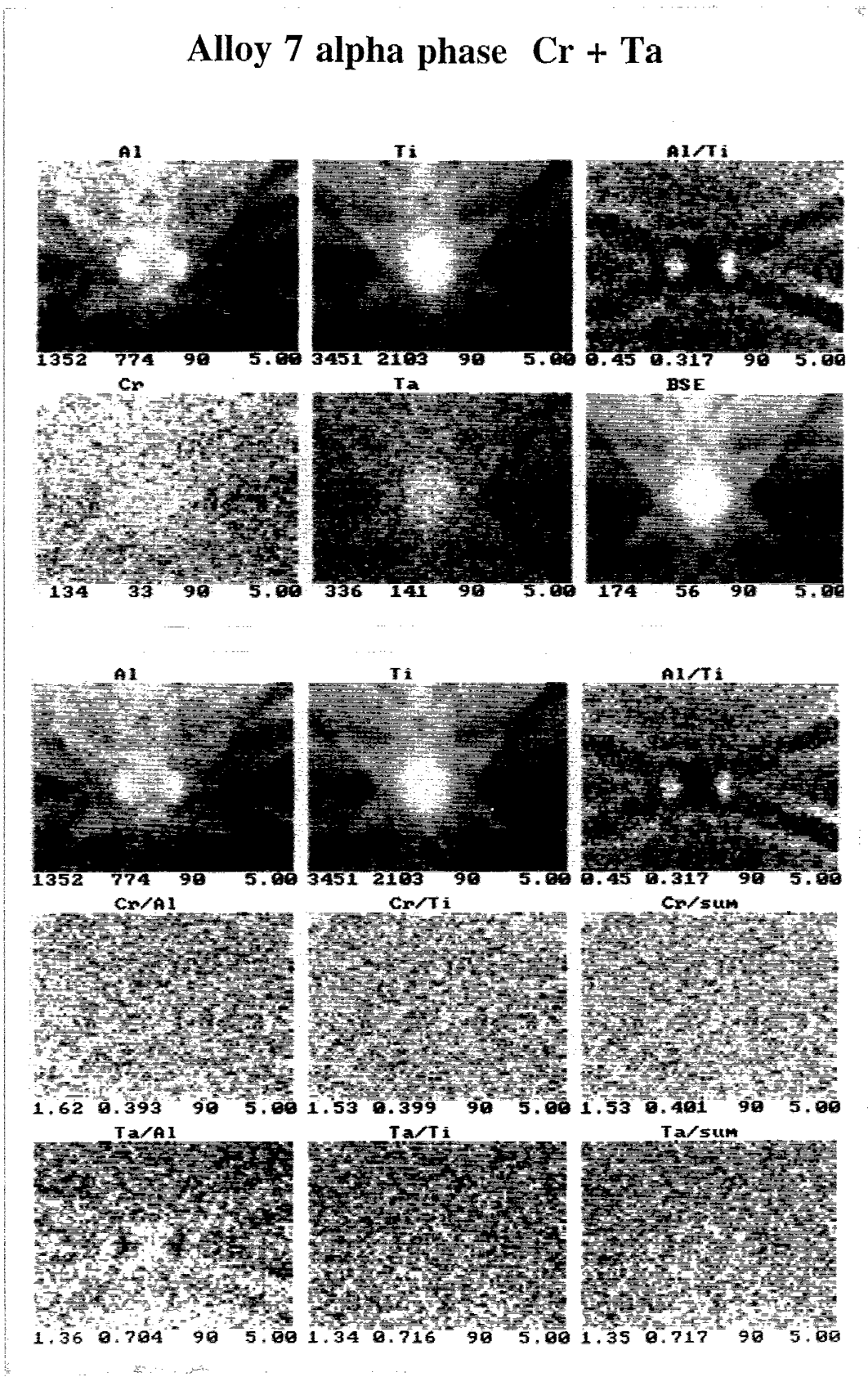

Fig.16. ICPs obtained from the $[\bar{1}\bar{1}23]$ zone axis of the α_2-phase of the Cr+Ta quaternary alloy (alloy 7).

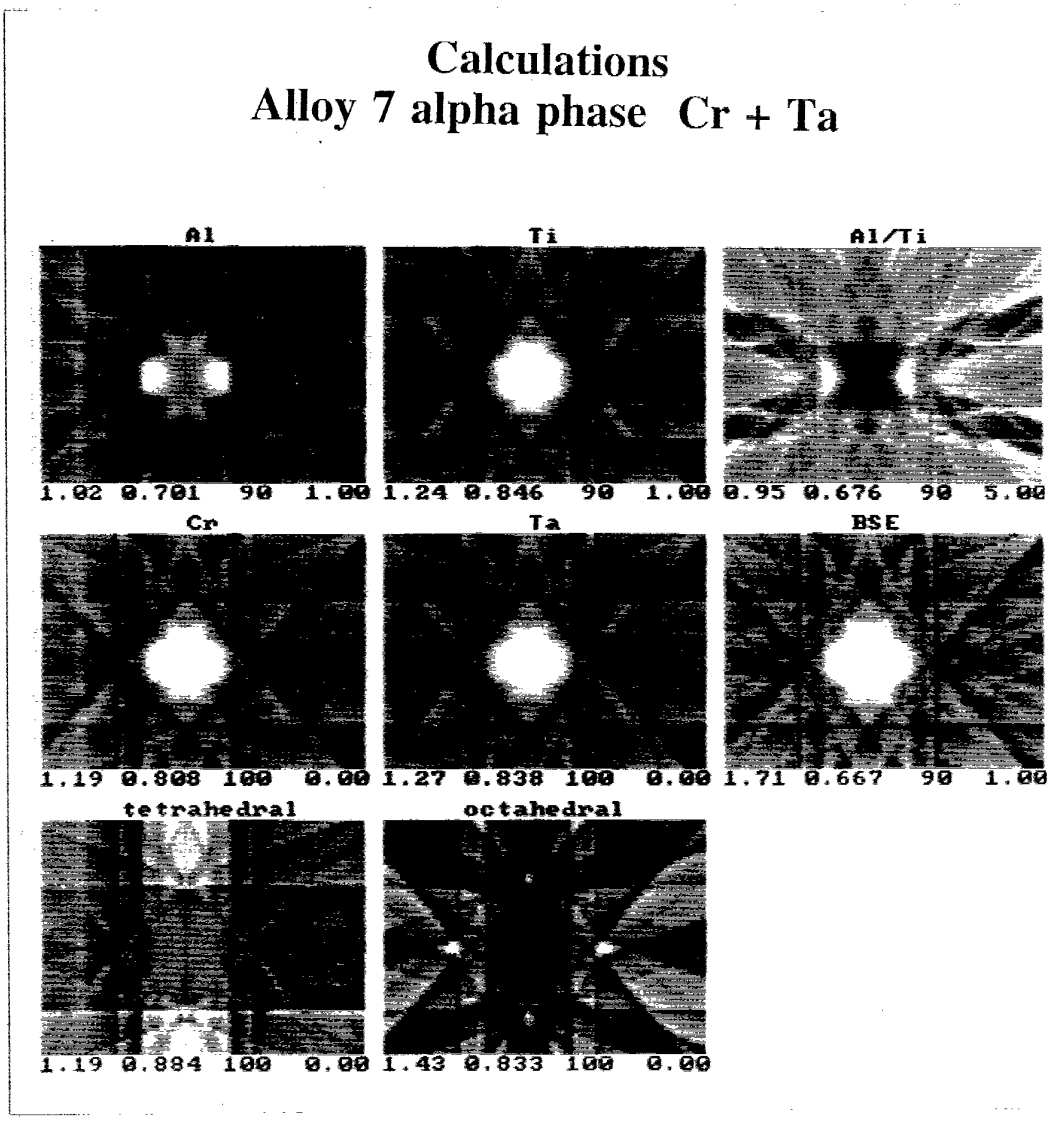

Fig.17. Calculated [$\bar{1}\bar{1}$23] ICPs for the α_2-phase of the Cr+Ta quaternary alloy, tilt $\phi = 15°$.

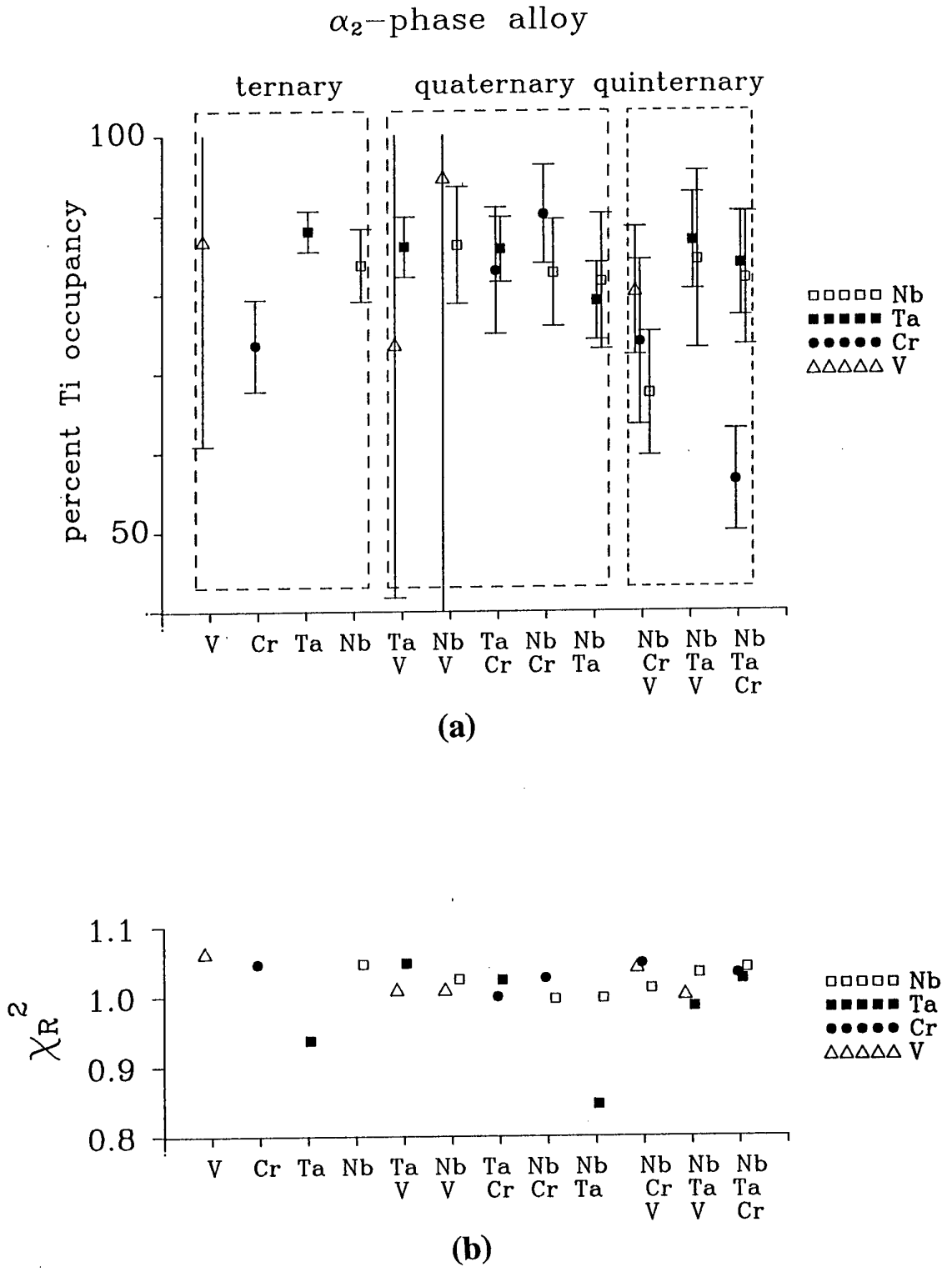

Fig.18. (a) Distribution of ternary, quaternary and quinternary alloying atoms on Ti sites in the α_2-phase (error bars indicate one standard deviation) and (b) χ_R^2 obtained from analyses.

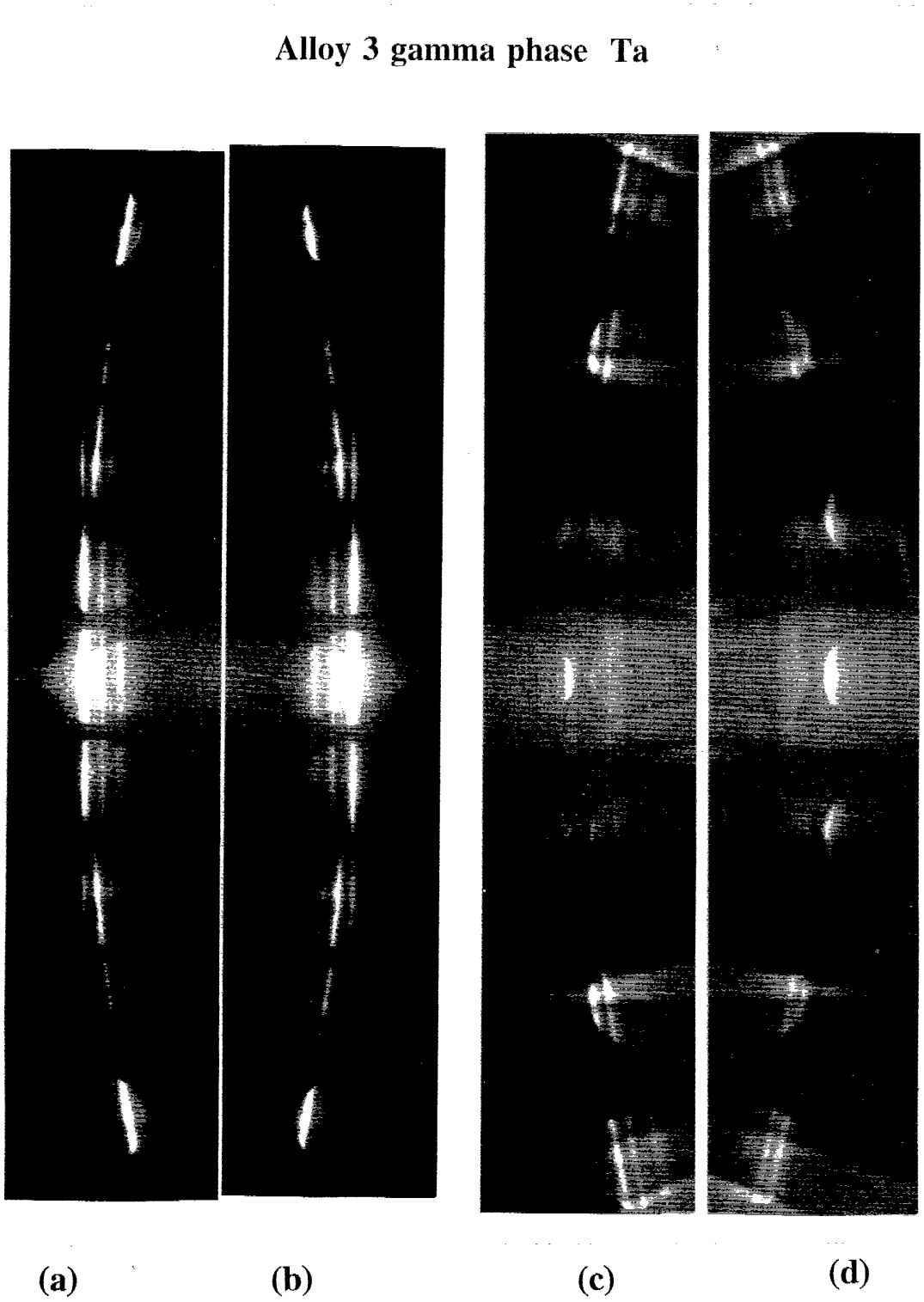

Fig. 19. (i)

Fig.19. Experimental n = 2 HOLZ reflections for an incident electron beam parallel to [110] in the γ-phase of (i) ternary Ta alloy (alloy 3), (ii) quaternary Cr+Nb alloy (alloy 8) and (iii) quinternary Cr+Ta+Nb alloy (alloy 12). (a) is centred about the $\bar{1}\bar{6}$ 14 0 reflection with (b) centred about the refection diametrically opposite $\bar{1}\bar{6}$ 14 0. (c) is centred about the $\bar{1}$ $\bar{1}$ 21 reflection with (d) centred about the refection diametrically opposite $\bar{1}$ $\bar{1}$ 21.

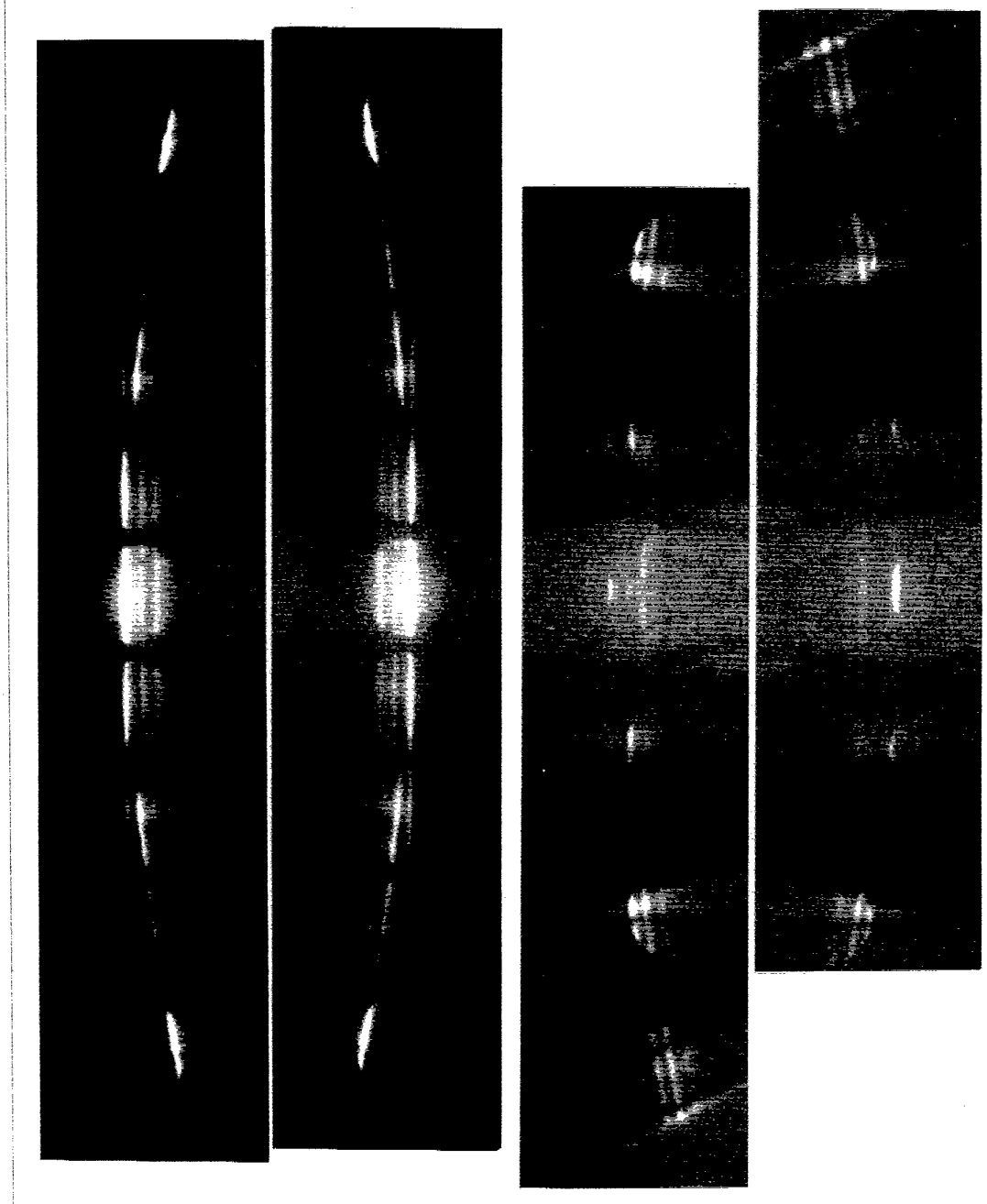

Fig. 19. (ii)

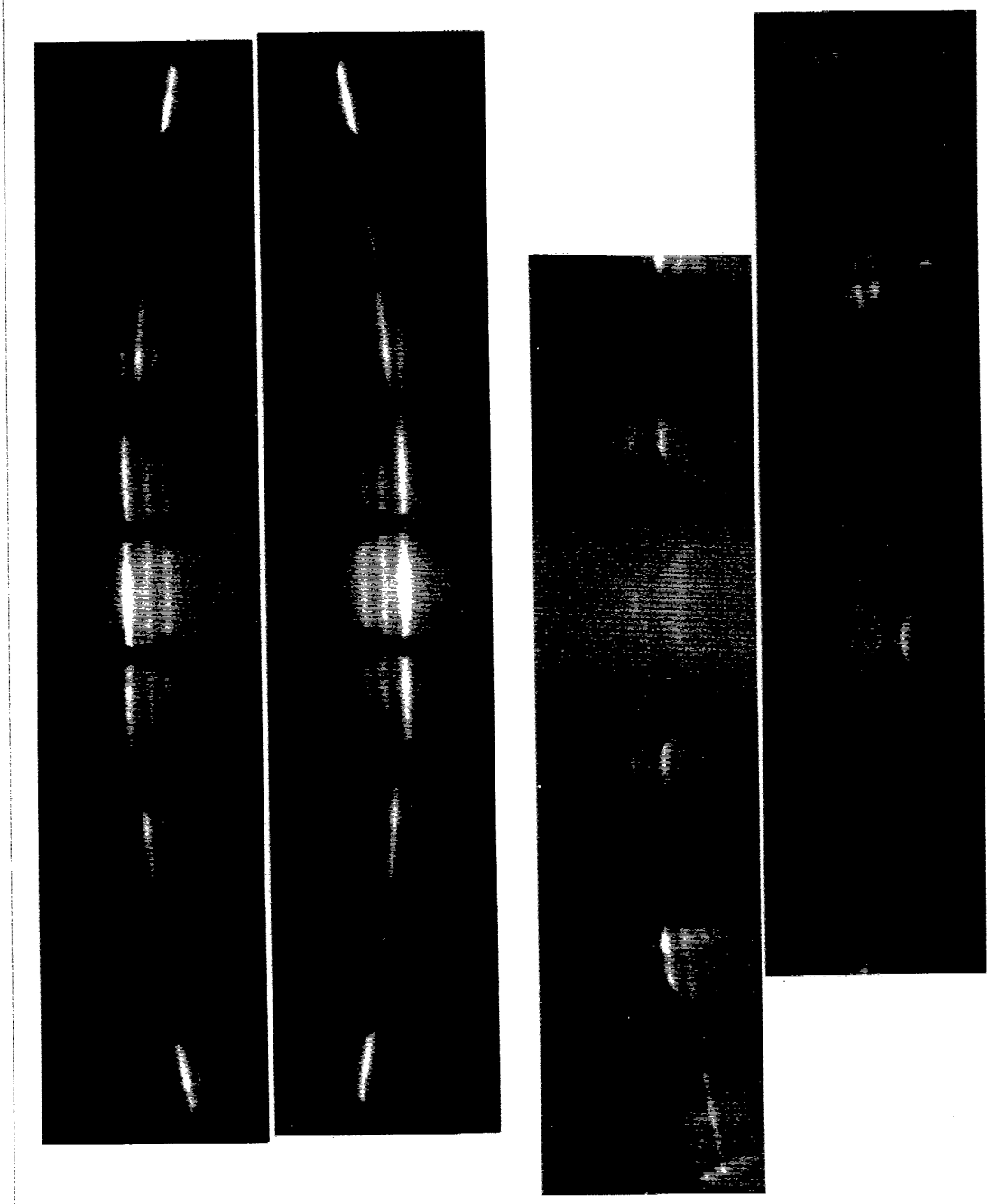

Fig. 19. (iii)

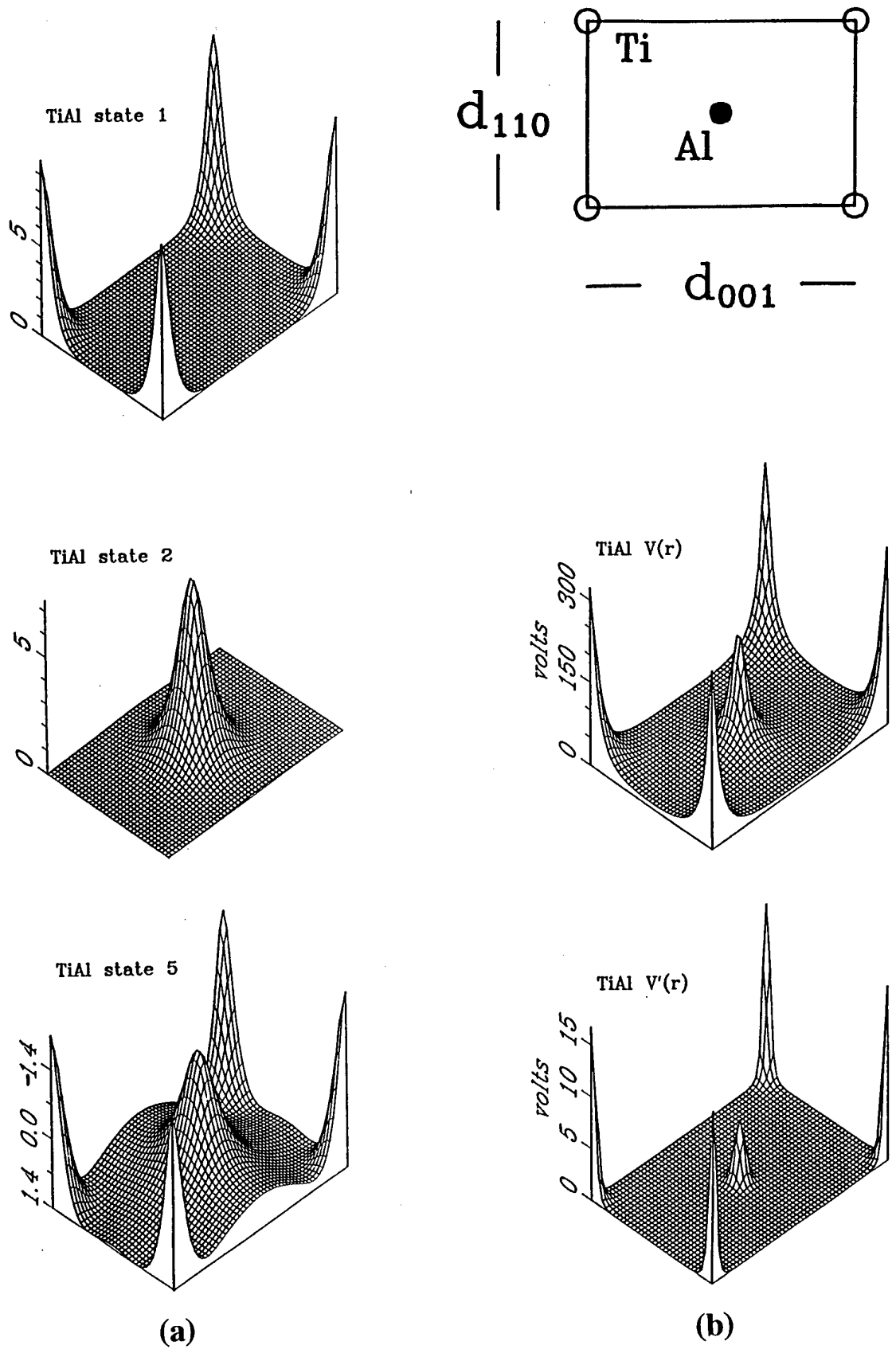

Fig.20. (a) $\phi^{(i)}(\mathbf{r})$ for i = 1, 2, and 5 for the γ-phase. (b) Projected [110] atomic structure with projected [110] elastic potential V(**r**) and projected [110] TDS potential V'(**r**) for the γ-phase.

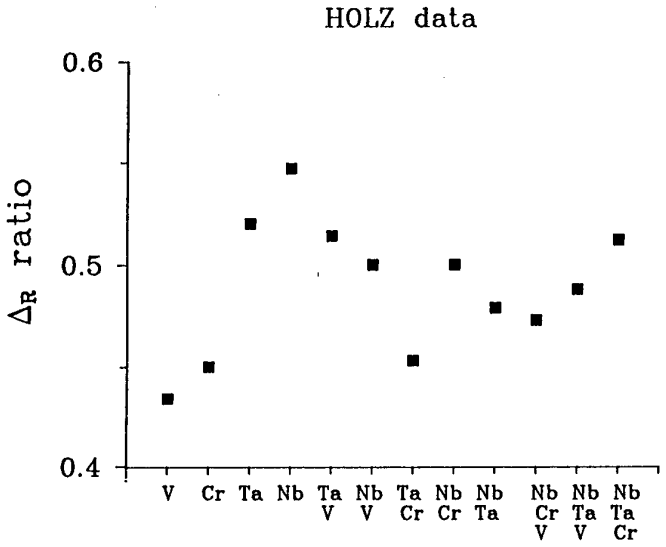

Fig.21. Experimentally measured ratios Δ_R of the separations $\Delta_{12} : \Delta_{15}$ for the HOLZ rings in the $\overline{1}6$ 14 0 refection for all 12 alloys.

APPENDIX A

Analysis of TiAl alloys with alloying elements

Measured k(X-Ti) or k-factors fully absorption corrected

Percentages in atomic percent

Thicknesses t in Angstroms

Standard tilt angle 20°

1. k-factors and interaction half-widths b_y in Å

k(Al) = 1.41	b = 0.1417
k(Ti) = 1.00	b = 0.0565
k(V) = 0.956	b = 0.0525
k(Cr) = 1.04	b = 0.0488
k(Ta) = 0.799	b = 0.0294
k(Nb) = 1.19	b = 0.0208

2. X-ray mean free path λ_y in microns

γ phase

Al	1.872
Ti	21.02
V	6.46
Cr	8.19
Ta	40.3
Nb	201

α_2 phase

Al	1.692
Ti	22.51
V	5.79
Cr	7.33
Ta	39.8
Nb	180

1. V

gamma phase

t = 789

	counts	%
Al	102582	48.8
Ti	148853	48.9
V	7168	2.26

Alloy 1 V
Gamma

Fitted constants for 1 V are:
Host 1 Al 0.54231E-02 ± 0.27484E-03
Host 2 Ti 0.27943E-02 ± 0.19600E-03
Constant -13.616 ± 1.0152
ChiSq = 4584.911
Chi2R = 1.001
Degrees of freedom = 4579
V
Host 1 Al % f = 53.376 ± 3.053
Host 2 Ti % f = 46.624 ± 2.671

alpha 2 phase

t = 1124

	counts	%
Al	115412	40.2
Ti	235835	55.8
V	17376	3.97

Alloy 1 V
Alpha

Fitted constants for 1 V are:
Host 1 Al 0.16899E-02 ± 0.18708E-02
Host 2 Ti 0.48723E-02 ± 0.84831E-03
Constant 0.48893E-06 ± 0.31339E-06
ChiSq = 4867.528
Chi2R = 1.063
Degrees of freedom = 4579
V
Host 1 Al % f = 13.214 ± 10.504
Host 2 Ti % f = 86.786 ± 25.796

2. Cr

gamma phase

t = 1580

	counts	%
Al	130866	47.8
Ti	202579	49.6
Cr	10342	2.66

Alloy 2 Cr
Gamma

Fitted constants for 1 Cr are:
Host 1 Al 0.68045E-01 ± 0.14825E-02
Host 2 Ti 0.16153E-01 ± 0.79907E-03
Constant -40.306 ± 4.1164
ChiSq = 4603.800
Chi2R = 1.005
Degrees of freedom = 4579
Cr
Host 1 Al % f = 69.005 ± 2.101
Host 2 Ti % f = 30.995 ± 1.079

alpha 2 phase

t = 1990

	counts	%
Al	105474	36.2
Ti	261576	58.9
Cr	20415	4.85

Alloy 2 Cr
Alpha

Fitted constants for 1 Cr are:
Host 1 Al 0.44896E-01 ± 0.69886E-02
Host 2 Ti 0.51105E-01 ± 0.29378E-02
Constant 45.832 ± 8.0367
ChiSq = 3220.832
Chi2R = 1.046
Degrees of freedom = 3078
Cr
Host 1 Al % f = 26.539 ± 2.544
Host 2 Ti % f = 73.461 ± 5.974

3. Ta

gamma phase

t = 984

	counts	%
Al	102892	48.1
Ti	152752	48.9
Ta	6488	3.05

Alloy 3 Ta
Gamma

Fitted constants for 1 Ta are:
Host 1 Al 0.44621E-01 ± 0.18074E-02
Host 2 Ti 0.12134 ± 0.15590E-02
Constant -66.254 ± 7.6483
ChiSq = 4787.505
Chi2R = 1.046
Degrees of freedom = 4579
Ta
Host 1 Al % f = 18.064 ± 0.561
Host 2 Ti % f = 81.936 ± 1.560

alpha 2 phase

t = 860

	counts	%
Al	74021	39.6
Ti	154308	56.5
Ta	13397	3.92

Alloy 3 Ta
Alpha

Fitted constants for 1 Ta are:
Host 1 Al 0.77252E-01 ± 0.86511E-02
Host 2 Ti 0.14676 ± 0.27389E-02
Constant -9.1971 ± 4.8997
ChiSq = 4290.034
Chi2R = 0.937
Degrees of freedom = 4579
Ta
Host 1 Al % f = 12.140 ± 1.010
Host 2 Ti % f = 87.860 ± 2.648

4. Nb

gamma phase

t = 816

	counts	%
Al	85614	48.6
Ti	123273	48.2
Nb	7016	3.26

Alloy 4 Nb
Gamma

Fitted constants for 1 Nb are:
Host 1 Al 0.18600E-02 ± 0.99794E-03
Host 2 Ti 0.56502E-01 ± 0.50440E-03
Constant 11.158 ± 2.3110
ChiSq = 4700.587
Chi2R = 1.027
Degrees of freedom = 4579
Nb
Host 1 Al % f = 1.839 ± 0.951
Host 2 Ti % f = 98.161 ± 1.970

alpha 2 phase

t = 764

	counts	%
Al	69049	39.2
Ti	147795	57.7
Nb	6723	3.12

Alloy 4 Nb
Alpha

Fitted constants for 1 Nb are:
Host 1 Al 0.36972E-01 ± 0.56855E-02
Host 2 Ti 0.52716E-01 ± 0.18771E-02
Constant 13.146 ± 3.0191
ChiSq = 4790.622
Chi2R = 1.046
Degrees of freedom = 4579
Nb
Host 1 Al % f = 16.431 ± 1.729
Host 2 Ti % f = 83.569 ± 4.622

5. V and Ta

gamma phase

t = 730

	counts	%
Al	105103	47.4
Ti	160224	49.9
V	3469	1.04
Ta	6488	1.62

Alloy 5 V Ta
Gamma

Fitted constants for 1 V are:
Host 1 Al 0.39100E-02 ± 0.37379E-03
Host 2 Ti 0.25206E-03 ± 0.20210E-03
Constant 0.51720E-06 ± 0.35539E-07
ChiSq = 4956.973
Chi2R = 1.083
Degrees of freedom = 4579
Fitted constants for 2 Ta are:
Host 1 Al 0.31662E-02 ± 0.78809E-03
Host 2 Ti 0.38643E-01 ± 0.42706E-03
Constant 0.28297E-05 ± 0.72803E-07
ChiSq = 4966.119
Chi2R = 1.085
Degrees of freedom = 4579
V
Host 1 Al % f = 89.376 ± 16.467
Host 2 Ti % f = 10.624 ± 6.942
Ta
Host 1 Al % f = 4.255 ± 0.973
Host 2 Ti % f = 95.745 ± 2.219

alpha 2 phase

t = 873

	counts	%
Al	80789	37.5
Ti	184620	58.7
V	5542	1.70
Ta	8379	2.13

Alloy 5 V Ta
Alpha

Fitted constants for 1 V are:
Host 1 Al 0.19454E-02 ± 0.15509E-02
Host 2 Ti 0.23411E-02 ± 0.72058E-03
Constant -5.1670 ± 1.4649
ChiSq = 4623.791
Chi2R = 1.010
Degrees of freedom = 4580
Fitted constants for 2 Ta are:
Host 1 Al 0.27313E-01 ± 0.40754E-02
Host 2 Ti 0.72056E-01 ± 0.18957E-02
Constant -27.247 ± 3.8704
ChiSq = 4794.020
Chi2R = 1.047
Degrees of freedom = 4580
V
Host 1 Al % f = 26.411 ± 13.375Host 2 Ti % f = 73.589 ± 31.904
Ta
Host 1 Al % f = 14.069 ± 1.488
Host 2 Ti % f = 85.931 ± 3.799

6. V and Nb

gamma phase

t = 1000

	counts	%
Al	95889	48.0
Ti	144134	49.1
V	3409	1.12
Nb	4365	1.77

Alloy 6 V Nb
Gamma

Fitted constants for V are:
Host 1 Al 0.12250E-01 ± 0.59137E-03
Host 2 Ti 0.66796E-02 ± 0.31101E-03
Constant -52.097 ± 2.7087
ChiSq = 4643.891
Chi2R = 1.014
Degrees of freedom = 4579
Fitted constants for Nb are:
Host 1 Al 0.68645E-02 ± 0.69688E-03
Host 2 Ti 0.37483E-01 ± 0.37456E-03
Constant -30.766 ± 3.2311
ChiSq = 4943.110
Chi2R = 1.080
Degrees of freedom = 4579
V
Host 1 % f = 47.283 ± 2.150
Host 2 % f = 52.717 ± 2.397
Nb
Host 1 % f = 8.220 ± 0.712
Host 2 % f = 91.780 ± 1.757

alpha 2 phase

t = 1200

	counts	%
Al	89596	40.6
Ti	180316	55.7
V	6396	1.91
Nb	4661	1.72

Alloy 6 V Nb
Alpha

Fitted constants for 1 V are:
Host 1 Al 0.42629E-03 ± 0.25846E-02
Host 2 Ti 0.25808E-02 ± 0.94601E-03
Constant -0.18909 ± 0.26874
ChiSq = 4622.970
Chi2R = 1.010
Degrees of freedom = 4579
Fitted constants for 2 Nb are:
Host 1 Al 0.11295E-01 ± 0.32794E-02
Host 2 Ti 0.23575E-01 ± 0.12006E-02
Constant 0.95975 ± 0.34318
ChiSq = 4690.147
Chi2R = 1.024
Degrees of freedom = 4579
V
Host 1 Al % f = 5.2680 ± 27.949
Host 2 Ti % f = 94.732 ± 65.321
Nb
Host 1 Al % f = 13.891 ± 2.873
Host 2 Ti % f = 86.109 ± 7.388

7. Cr and Ta

gamma phase

t = 900

	counts	%
Al	78709	47.1
Ti	121739	50.1
Cr	2709	1.16
Ta	5057	1.66

Alloy 7 Cr Ta
Gamma

Fitted constants for 1 Cr are:
Host 1 Al 0.88692E-01 ± 0.24784E-02
Host 2 Ti 0.30869E-02 ± 0.10124E-02
Constant -3.6878 ± 0.85427
ChiSq = 4622.382
Chi2R = 1.009
Degrees of freedom = 4579
Fitted constants for 2 Ta are:
Host 1 Al 0.17118E-01 ± 0.23999E-02
Host 2 Ti 0.48018E-01 ± 0.98354E-03
Constant 0.60487 ± 0.84170
ChiSq = 4694.225
Chi2R = 1.025
Degrees of freedom = 4579
Cr
Host 1 Al % f = 90.358 ± 5.429
Host 2 Ti % f = 9.642 ± 2.597
Ta
Host 1 Al % f = 10.416 ± 1.210
Host 2 Ti % f = 89.584 ± 3.279

alpha 2 phase

t = 1100

	counts	%
Al	67442	42.7
Ti	123137	53.2
Cr	4471	2.02
Ta	6276	2.16

Alloy 7 Cr Ta
Alpha

Fitted constants for 1 Cr are:
Host 1 Al 0.15729E-01 ± 0.37449E-02
Host 2 Ti 0.25282E-01 ± 0.16672E-02
Constant 0.68453 ± 2.5732
ChiSq = 4573.991
Chi2R = 0.999
Degrees of freedom = 4579
Fitted constants for 2 Ta are:
Host 1 Al 0.34852E-01 ± 0.48642E-02
Host 2 Ti 0.68499E-01 ± 0.21678E-02
Constant -0.30042 ± 3.3500
ChiSq = 4682.404
Chi2R = 1.023
Degrees of freedom = 4579
Cr
Host 1 Al % f = 17.055 ± 2.822
Host 2 Ti % f = 82.945 ± 8.024
Ta
Host 1 Al % f = 14.395 ± 1.448
Host 2 Ti % f = 85.605 ± 4.117

8. Cr and Nb

gamma phase

t = 600

	counts	%
Al	86443	46.0
Ti	137516	50.9
Cr	3577	1.38
Nb	3911	1.72

Alloy 8 Cr Nb
Gamma

Fitted constants for 1 Cr are:
Host 1 Al 0.91493E-01 ± 0.19927E-02
Host 2 Ti 0.11399E-01 ± 0.10457E-02
Constant -31.173 ± 2.8106
ChiSq = 5002.768
Chi2R = 1.093
Degrees of freedom = 4579
Fitted constants for 2 Nb are:
Host 1 Al 0.56071E-02 ± 0.12753E-02
Host 2 Ti 0.36355E-01 ± 0.69433E-03
Constant -8.7839 ± 1.8475
ChiSq = 4463.221
Chi2R = 0.975
Degrees of freedom = 4579
Cr
Host 1 Al % f = 76.654 ± 2.990
Host 2 Ti % f = 23.346 ± 1.422
Nb
Host 1 Al % f = 5.935 ± 1.207
Host 2 Ti % f = 94.065 ± 3.343

alpha 2 phase

t = 600

	counts	%
Al	90083	40.0
Ti	181760	55.9
Cr	7598	2.45
Nb	4521	1.65

Alloy 8 Cr Nb
Alpha

Fitted constants for 1 Cr are:
Host 1 Al 0.12278E-01 ± 0.34907E-02
Host 2 Ti 0.34293E-01 ± 0.14667E-02
Constant 2.2129 ± 3.0285
ChiSq = 4698.530
Chi2R = 1.026
Degrees of freedom = 4579
Fitted constants for 2 Nb are:
Host 1 Al 0.13981E-01 ± 0.27363E-02
Host 2 Ti 0.20568E-01 ± 0.11500E-02
Constant 1.3828 ± 2.3758
ChiSq = 4561.201
Chi2R = 0.996
Degrees of freedom = 4579
Cr
Host 1 Al % f = 10.016 ± 2.233
Host 2 Ti % f = 89.984 ± 6.191
Nb
Host 1 Al % f = 17.447 ± 2.368
Host 2 Ti % f = 82.553 ± 6.752

9. Ta and Nb

gamma phase

t = 1100

	counts	%
Al	93611	46.7
Ti	146494	49.9
Ta	6052	1.64
Nb	4394	1.77

Alloy 9 Ta Nb
Gamma

Fitted constants for 1 Ta are:
Host 1 Al 0.10911E-01 ± 0.16272E-02
Host 2 Ti 0.45079E-01 ± 0.84325E-03
Constant 4.1245 ± 3.5092
ChiSq = 4952.446
Chi2R = 1.082
Degrees of freedom = 4579
Fitted constants for 2 Nb are:
Host 1 Al 0.16376E-02 ± 0.11439E-02
Host 2 Ti 0.28682E-01 ± 0.59322E-03
Constant -1.2318 ± 2.4797
ChiSq = 4627.133
Chi2R = 1.011
Degrees of freedom = 4579
Ta
Host 1 Al % f = 11.503 ± 1.375
Host 2 Ti % f = 88.497 ± 3.205
Nb
Host 1 Al % f = 2.975 ± 1.958
Host 2 Ti % f = 97.025 ± 4.338

alpha 2 phase

t = 650

	counts	%
Al	68397	36.7
Ti	160508	59.5
Ta	7193	2.13
Nb	3785	1.67

Alloy 9 Ta Nb
Alpha

Fitted constants for 1 Ta are:
Host 1 Al 0.40901E-01 ± 0.59009E-02
Host 2 Ti 0.62537E-01 ± 0.25429E-02
Constant 13.536 ± 2.1629
ChiSq = 3869.135
Chi2R = 0.845
Degrees of freedom = 4579
Fitted constants for 2 Nb are:
Host 1 Al 0.12379E-01 ± 0.33827E-02
Host 2 Ti 0.22189E-01 ± 0.14584E-02
Constant 8.1842 ± 1.2429
ChiSq = 4566.079
Chi2R = 0.997
Degrees of freedom = 4579
Ta
Host 1 Al % f = 21.038 ± 1.932
Host 2 Ti % f = 78.962 ± 4.947
Nb
Host 1 Al % f = 18.518 ± 3.318
Host 2 Ti % f = 81.482 ± 8.590

10. V, Cr and Nb

gamma phase

t = 1090

	counts	%
Al	97839	48.4
Ti	145464	49.1
V	1439	0.47
Cr	2749	0.97
Nb	2879	1.15

Alloy 10 V Cr Nb
Gamma

Fitted constants for 1 V are:
Host 1 Al 0.48077E-01 ± 0.91512E-03
Host 2 Ti 0.33951E-04 ± 0.31656E-03
Constant 0.74284E-05 ± 0.11394E-06
ChiSq = 4765.689
Chi2R = 1.041
Degrees of freedom = 4579
Fitted constants for 2 Cr are:
Host 1 Al 0.12500E-01 ± 0.69451E-03
Host 2 Ti 0.82525E-03 ± 0.24080E-03
Constant 0.19822E-05 ± 0.85076E-07
ChiSq = 5113.332
Chi2R = 1.117
Degrees of freedom = 4579
Fitted constants for 3 Nb are:
Host 1 Al 0.13568E-02 ± 0.89644E-03
Host 2 Ti 0.25790E-01 ± 0.31197E-03
Constant 0.25208E-05 ± 0.10286E-06
ChiSq = 4621.271
Chi2R = 1.009
Degrees of freedom = 4579
V
Host 1 Al % f = 99.794 ± 4.225
Host 2 Ti % f = 0.206 ± 1.915
Cr
Host 1 Al % f = 83.805 ± 8.399
Host 2 Ti % f = 16.195 ± 3.532
Nb
Host 1 Al % f = 1.766 ± 1.126
Host 2 Ti % f = 98.234 ± 2.561

alpha 2 phase

t = 500

	counts	%
Al	43136	39.7
Ti	88590	56.7
V	1451	0.89
Cr	2575	1.72
Nb	1408	1.07

Alloy 10 V Cr Nb
Alpha

Fitted constants for 1 V+Cr are:
Host 1 Al 0.14910E-01 ± 0.35189E-02
Host 2 Ti 0.24367E-01 ± 0.16035E-02
Constant -4.8288 ± 2.0074
ChiSq = 4770.220
Chi2R = 1.042
Degrees of freedom = 4579
Fitted constants for 2 Cr are:
Host 1 Al 0.75746E-02 ± 0.19280E-02
Host 2 Ti 0.85850E-02 ± 0.87987E-03
Constant -19.903 ± 1.0904
ChiSq = 4792.107
Chi2R = 1.047
Degrees of freedom = 4579
Fitted constants for 3 Nb are:
Host 1 Al 0.14519E-01 ± 0.24380E-02
Host 2 Ti 0.12034E-01 ± 0.11109E-02
Constant 4.9798 ± 1.3957
ChiSq = 4631.229
Chi2R = 1.011
Degrees of freedom = 4579
V+Cr
Host 1 Al % f = 19.737 ± 3.058
Host 2 Ti % f = 80.263 ± 8.108
Cr
Host 1 Al % f = 26.176 ± 4.285
Host 2 Ti % f = 73.824 ± 10.339
Nb
Host 1 Al % f = 32.654 ± 3.916
Host 2 Ti % f = 67.346 ± 7.842

11. V, Ta and Nb

gamma phase

t = 760

	counts	%
Al	114720	47.0
Ti	177240	50.1
V	2378	0.65
Ta	4475	1.01
Nb	3356	1.20

Alloy 11 V Ta Nb
Gamma

Fitted constants for 1 V are:
Host 1 Al 0.66629E-02 ± 0.82098E-03
Host 2 Ti 0.77902E-03 ± 0.41820E-03
Constant -6.0045 ± 0.57998
ChiSq = 4412.085
Chi2R = 0.998
Degrees of freedom = 4421
Fitted constants for 2 Ta are:
Host 1 Al 0.20469E-01 ± 0.16577E-02
Host 2 Ti 0.45357E-01 ± 0.84978E-03
Constant -9.8263 ± 1.1862
ChiSq = 4543.132
Chi2R = 1.028
Degrees of freedom = 4421
Fitted constants for 3 Nb are:
Host 1 Al 0.42466E-02 ± 0.10466E-02
Host 2 Ti 0.22693E-01 ± 0.53958E-03
Constant -0.39076 ± 0.75601
ChiSq = 4417.545
Chi2R = 0.999
Degrees of freedom = 4421
V
Host 1 Al % f = 81.378 ± 17.064
Host 2 Ti % f = 18.622 ± 7.248
Ta
Host 1 Al % f = 18.737 ± 1.104
Host 2 Ti % f = 81.263 ± 2.623
Nb
Host 1 Al % f = 8.727 ± 1.814
Host 2 Ti % f = 91.273 ± 4.297

alpha 2 phase

t = 738

	counts	%
Al	86514	38.0
Ti	193488	58.5
V	3849	1.12
Ta	5338	1.29
Nb	3208	1.15

Alloy 11 V Ta Nb
Alpha

Fitted constants for 1 V are:
Host 1 Al 0.15378E-01 ± 0.21712E-02
Host 2 Ti -0.39963E-02 ± 0.83000E-03
Constant -0.70576 ± 0.62156
ChiSq = 4592.457
Chi2R = 1.003
Degrees of freedom = 4579
Fitted constants for 2 Ta are:
Host 1 Al 0.31296E-01 ± 0.58150E-02
Host 2 Ti 0.45187E-01 ± 0.22223E-02
Constant -3.3951 ± 1.6668
ChiSq = 4510.530
Chi2R = 0.985
Degrees of freedom = 4579
Fitted constants for 3 Nb are:
Host 1 Al 0.11466E-01 ± 0.34300E-02
Host 2 Ti 0.13594E-01 ± 0.13110E-02
Constant 7.4890 ± 0.98319
ChiSq = 4728.643
Chi2R = 1.033
Degrees of freedom = 4579
V
Host 1 Al % f = -598.60 ± 1947.924
Host 2 Ti % f = 698.604 ± 2252.372
Ta
Host 1 Al % f = 13.362 ± 1.877
Host 2 Ti % f = 86.638 ± 6.058
Nb
Host 1 Al % f = 15.812 ± 3.497
Host 2 Ti % f = 84.188 ± 11.199

12. Cr, Ta and Nb

gamma phase

t = 1216

	counts	%
Al	86655	47.6
Ti	132774	49.6
Cr	2224	0.87
Ta	2771	0.83
Nb	2509	1.11

Alloy 12 Cr Ta Nb
Gamma

Fitted constants for 1 Cr are:
Host 1 Al 0.38454E-01 ± 0.59140E-03
Host 2 Ti -0.58702E-03 ± 0.28349E-03
Constant -13.732 ± 1.2033
ChiSq = 4806.191
Chi2R = 1.050
Degrees of freedom = 4579
Fitted constants for 2 Ta are:
Host 1 Al 0.77260E-02 ± 0.75951E-03
Host 2 Ti 0.37826E-01 ± 0.37994E-03
Constant -21.306 ± 1.5645
ChiSq = 4467.900
Chi2R = 0.976
Degrees of freedom = 4579
Fitted constants for 3 Nb are:
Host 1 Al 0.33176E-02 ± 0.49454E-03
Host 2 Ti 0.20415E-01 ± 0.24786E-03
Constant -7.6694 ± 1.0204
ChiSq = 4011.098
Chi2R = 0.876
Degrees of freedom = 4579
Cr
Host 1 Al % f = 102.926 ± 3.475
Host 2 Ti % f = -2.926 ± 1.498
Ta
Host 1 Al % f = 9.884 ± 0.801
Host 2 Ti % f = 90.116 ± 1.824
Nb
Host 1 Al % f = 8.026 ± 1.021
Host 2 Ti % f = 91.974 ± 2.305

alpha 2 phase

t = 1338

	counts	%
Al	63352	39.0
Ti	138860	57.5
Cr	3317	1.44
Ta	3332	1.10
Nb	2072	1.02

Alloy 12 Cr Ta Nb
Alpha

Fitted constants for 1 Cr are:
Host 1 Al 0.21696E-01 ± 0.28521E-02
Host 2 Ti 0.10686E-01 ± 0.10851E-02
Constant 0.40994E-05 ± 0.76377E-07
ChiSq = 4725.167
Chi2R = 1.032
Degrees of freedom = 4579
Fitted constants for 2 Ta are:
Host 1 Al 0.12970E-01 ± 0.30543E-02
Host 2 Ti 0.25275E-01 ± 0.11620E-02
Constant 0.59662E-05 ± 0.84604E-07
ChiSq = 4688.161
Chi2R = 1.024
Degrees of freedom = 4579
Fitted constants for 3 Nb are:
Host 1 Al 0.85760E-02 ± 0.23766E-02
Host 2 Ti 0.14688E-01 ± 0.90418E-03
Constant 0.35656E-05 ± 0.63017E-07
ChiSq = 4763.654
Chi2R = 1.040
Degrees of freedom = 4579
Cr
Host 1 Al % f = 43.596 ± 4.950
Host 2 Ti % f = 56.404 ± 6.379
Ta
Host 1 Al % f = 16.344 ± 2.595
Host 2 Ti % f = 83.656 ± 6.552
Nb
Host 1 Al % f = 18.187 ± 3.294
Host 2 Ti % f = 81.813 ± 8.371